COMPATIBILITY OF URANIUM-PLUTONIUM CARBIDE FUELS AND POTENTIAL LMFBR CLADDING MATERIALS

T. W. Latimer

U of C-AUA-USAEC

ARGONNE NATIONAL LABORATORY, ARGONNE, ILLINOIS

DISCLAIMER

Printed in the United States of America
Available from
National Technical Information Service
U.S. Department of Commerce
5285 Port Royal Road
Springfield, Virginia 22151
Price: Printed Copy $3.00; Microfiche $0.95

ANL-7827
Metals, Ceramics,
and Materials

ARGONNE NATIONAL LABORATORY
9700 South Cass Avenue
Argonne, Illinois 60439

COMPATIBILITY OF URANIUM-PLUTONIUM CARBIDE FUELS AND POTENTIAL LMFBR CLADDING MATERIALS

by

T. W. Latimer

Materials Science Division

September 1971

TABLE OF CONTENTS

LIST OF FIGURES

LIST OF FIGURES

LIST OF TABLES

COMPATIBILITY OF URANIUM-PLUTONIUM CARBIDE FUELS AND POTENTIAL LMFBR CLADDING MATERIALS

by

T. W. Latimer

ABSTRACT

The contact compatibility (in the absence of sodium) between (U,Pu)C with equivalent carbon contents of 4.83, 5.25, and 6.75 wt % and various iron-, nickel-, and vanadium-base alloys was studied at 700-1100°C for 168-4000 hr. Austenitic iron-base alloys, containing 25 wt % or less nickel and tested at 800°C for up to 4000 hr, showed little or no evidence of carbon transfer from stoichiometric or hyperstoichiometric $(U_{0.8}Pu_{0.2})C$ that contained up to 20 vol % $(U,Pu)_2C_3$. Three austenitic alloys containing more than 30 wt % nickel reacted with stoichiometric and hyperstoichiometric $(U_{0.8}Pu_{0.2})C$ to form intermetallic compounds at the fuel-cladding interface and precipitates in the cladding at 700 and 800°C. Vanadium-base alloys containing 15-20 wt % titanium were carburized by $(U_{0.8}Pu_{0.2})C$ and reduced $(U,Pu)_2C_3$ to (U,Pu)C at 800°C. However, alloys containing 5 wt % or less titanium or other relatively strong carbide formers were only slightly affected by hyperstoichiometric (U,Pu)C at 800°C for up to 4000 hr.

I. INTRODUCTION

The chemical compatibility of the fuel and cladding is extremely important to the lifetime of nuclear-reactor fuel elements. The formation of new phases at the fuel-cladding interface or other changes in the alloy chemistry of the cladding material can significantly affect the load-bearing capacity of the cladding. A knowledge of the changes that occur near the fuel-cladding interface can be used as a guide in the development of potential cladding materials as well as in the selection of available materials before irradiation testing.

Uranium-plutonium monocarbide is a promising fuel material because it possesses favorable characteristics of metal density, thermal conductivity, and melting point. However, close control of the carbon content is necessary to produce material that contains only the monocarbide phase and eliminates higher carbide phases that degrade the favorable

properties. Maintaining a single-phase structure is further complicated by (1) contamination of finely divided (U,Pu)C powder by oxygen and nitrogen during fabrication procedures, and (2) the relative ease by which oxygen and nitrogen can substitute for carbon in the monocarbide lattice. Because of oxygen and nitrogen contamination during fabrication, hyperstoichiometric (U,Pu)C is frequently the end product. The higher carbide phase usually found in hyperstoichiometric $(U_{0.8}Pu_{0.2})C$ is $(U,Pu)_2C_3$. However, hyperstoichiometric UC, if not subjected to long heat treatments, predominantly contains UC_2 as the higher carbide phase, even though this phase is metastable below 1500°C for uranium-carbon mixtures containing between 50 and 60 at. % carbon. Because of this difference in second phase, estimates of the compatibility of uranium-plutonium carbide compositions based on uranium carbide data are generally unreliable.

In the present investigation, the contact compatibility (i.e., without a sodium bond) of both stoichiometric and slightly hyperstoichiometric (U,Pu)C was tested out of pile with potential cladding materials. In addition, a composition of predominantly $(U,Pu)_2C_3$ was used to a limited extent to interpret the results of the tests of hyperstoichiometric (U,Pu)C. The potential cladding materials (iron-, nickel-, and vanadium-base alloys) were selected primarily for commercial availability and high creep-rupture strengths.

II. MATERIALS

A. Cladding Materials

The iron-base alloys tested were Types 304 and 316 stainless steel, Timken 16-15-6 and 16-25-6, and Haynes 56. The nickel-base alloys were Incoloy 800, Hastelloy-X, and Inconel 625. The nominal compositions of these alloys, which were purchased from commercial vendors, are given in Table I. Vanadium alloys V-20 wt % Ti, V-15 wt % Ti-7.5 wt % Cr, V-15 wt % Cr-5 wt % Ti, and V-10 wt % Cr were prepared at ANL by the

TABLE I. Composition and Creep-rupture Data of Potential Cladding Alloys

Alloy	Creep-rupture Stress,[a] for Failure in 10^4 hr at 700°C, psi	Composition, wt %						
		Fe	Ni	Cr	Mo	Mn	Co	Other
304 SS	9,000	68	9	19	-	2	-	2
316 SS	11,000	64	13	17	2.5	2	-	1.5
16-15-6	15,000	55	15	16	6	7.5	-	0.9
16-25-6	14,000	50	25	16	6	1.3	-	0.9
Haynes 56	22,000	45	13	21	4.5	1.5	11.5	3.5
Incoloy 800	11,000	46	32	21	-	0.75	-	0.4
Hastelloy-X	15,000	18	48	22	9	1	1.5	1.1
Inconel 625	30,000	3	61	22	9	0.15	-	4.8

[a]Extrapolated and estimated where adequate data do not exist.

Fabrication Technology Group. VANSTAR-7, -8, and -9 alloys were prepared by the Westinghouse Electric Corporation Advanced Reactors Division. The chemical analyses of all vanadium-base alloys tested are listed in Table II.

TABLE II. Chemical Analyses of Vanadium Alloys

Alloy	Ti, wt %	Cr, wt %	Fe, wt %	Ta, wt %	Nb, wt %	Zr, wt %	O, ppm	N, ppm	H, ppm	C, ppm	V
V-20 wt % Ti	19.0	-	-	-	-	-	720	147	35	198	Balance
V-15 wt % Ti-7.5 wt % Cr	14.8	7.5	-	-	-	-	702	400	14	250	Balance
V-15 wt % Cr-5 wt % Ti	5.5	14.4	-	-	-	-	900	250	13	280	Balance
V-10 wt % Cr	-	10.2	-	-	-	-	705	280	22	310	Balance
VANSTAR-7	-	8.8	3.1	-	-	1.2	620	79	NA	560	Balance
VANSTAR-8	-	8.7	-	9.7	-	1.1	540	68	NA	500	Balance
VANSTAR-9	-	-	6.3	-	5.2	1.3	590	79	NA	500	Balance

B. Carbide Specimens

Three carbide fuel compositions, each having an overall uranium-to-plutonium ratio of 4:1, were tested: 4.83 wt % equivalent carbon (single-phase (U,Pu)C), 5.25 wt % equivalent carbon (approximately 20% $(U,Pu)_2C_3$), and 6.75 wt % equivalent carbon (approximately 90% $(U,Pu)_2C_3$). Although both compositions containing the sesquicarbide phase had the same uranium-to-plutonium ratio, the plutonium content of this phase in the two compositions was not equal. The plutonium content of the sesquicarbide phase in the 5.25 wt % carbon composition was found by electron-microprobe analysis to be 1.9 times that of the monocarbide matrix.

Arc-melted buttons of the desired composition were crushed to -44-μ powder in gloveboxes that contained an inert atmosphere if nitrogen with impurities of oxygen and water vapor of about 50 and 100 ppm, respectively. The powder was coated with 0.5 wt % Carbowax binder and pressed into pellets at a pressure of 60,000 psi. The as-pressed pellets were 0.273 in. in diameter by approximately 0.2 in. in length. The pellets were sintered in a tantalum-element resistance furnace under a flowing argon atmosphere (~1 liter/min) and were held at the sintering temperatures for 3 hr. The sintering temperatures and densities of the three compositions are listed in Table III.

TABLE III. Compositions and Sintered Densities of (U,Pu) Carbide Pellets Used for Compatibility Tests

Equivalent Carbon, wt %	C, wt %	O_2, ppm	N_2, ppm	Sintering Temperature, °C	Density, g/ml	Theoretical Density, %
4.83	4.74	900	300	1900	11.67	86
5.25	5.10	800	1000	1850	11.28	84
6.75	6.73	80	100	1800	11.90	92

III. TEST MATRIX

Primarily, two temperatures and two heat-treatment periods were used in the compatibility tests. The principal test temperatures were 700 and 800°C, but some tests were conducted at 900, 950, and 1100°C. Primarily, the tests were conducted for 1000 and 4000 hr. The test matrix for all cladding and fuel combinations tested is given in Table IV.

TABLE IV. Carbide Compatibility Test Matrix

	Carbide Fuel Composition					
	4.83 wt % C		5.25 wt % C		6.75 wt % C	
Cladding Alloy	°C	Hr	°C	Hr	°C	Hr
304 SS	800	1000	800	1000	800	1000
	800	4000	800	4000	-	-
	1100	400	-	-	-	-
	1100	1000	-	-	-	-
316 SS	800	1000	800	1000	800	1000
	800	4000	800	4000	-	-
16-25-6	800	1000	800	1000	800	1000
	-	-	800	4000	-	-
16-15-6	800	1000	800	1000	-	-
Haynes 56	800	1000	800	1000	800	1000
	800	4000	800	4000	-	-
	900	1000	900	1000	-	-
Incoloy 800	700	1000	-	-	800	1000
	800	1000	-	-	-	-
Hastelloy-X	700	1000	700	1000	700	1000
	800	1000	800	1000	800	1000
Inconel 625	700	1000	700	1000	700	1000
	800	1000	800	1000	800	1000
V-20 wt % Ti	700	1000	700	1000	-	-
	800	1000	-	-	-	-
	950	168	-	-	-	-
	950	1000	-	-	-	-
V-15 wt % Ti-7.5 wt % Cr	800	1000	800	1000	800	1000
V-15 wt % Cr-5 wt % Ti	800	1000	800	1000	-	-
	-	-	800	4000	-	-
V-10 wt % Cr	800	1000	800	1000	800	1000
	-	-	800	4000	-	-
VANSTAR-7	-	-	800	1000	-	-
VANSTAR-8	-	-	800	1000	-	-
	-	-	800	4000	-	-
VANSTAR-9	-	-	800	1000	-	-
	-	-	800	4000	-	-

IV. EXPERIMENTAL PROCEDURE

Each compatibility assembly consisted of a pellet of the carbide fuel between two disks of cladding material held in contact by means of a molybdenum frame. In addition, a third metal disk of Type 304 stainless steel was added to the assembly to make the total length of pellets in the assembly 0.65-0.70 in. (see Fig. 1). The high strength and smaller linear thermal-expansion coefficient of the molybdenum holder were found to be effective in maintaining good contact between fuel and cladding materials during the test.

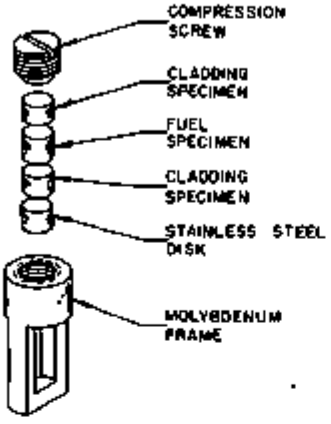

Fig. 1

Compatibility Test Assembly. Neg. No. MSD-54778.

Approximately 0.5 mm was ground off each end of the carbide pellets to minimize the chance of surface-impurity phases. The fuel-cladding contact surfaces were then polished flat with 4/0 emery paper on a glass plate using a special specimen holder shown in Fig. 2. Immediately after polishing, the specimens were assembled and pressure was applied by means of a screw in one end of the molybdenum holder. The assembly was then placed in a capsule, evacuated, backfilled with one-third atmosphere of helium, and sealed. Quartz capsules were used for most of the tests, although stainless steel capsules were used for the 4000-hr tests.

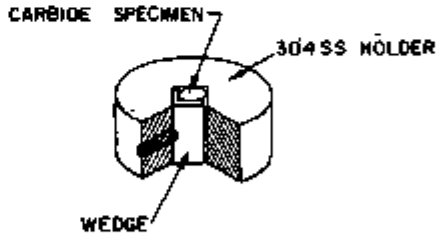

Fig. 2

Specimen Holder for Polishing Carbide Fuel Specimens. Neg. No. MSD-54779.

After being removed from their capsules, the couples were mounted in a polyester resin. This method was chosen because of the danger of breaking the fuel-cladding bond by mounting in Bakelite. Longitudinal sections were then prepared by grinding through series 120- to 600-grit grinding paper. Polishing was done with 6-μ diamond paste on AB Texmet* paper, and 1-μ diamond paste on AB Microcloth.* Hyprez* lubricant was used throughout the grinding and polishing procedure.

The iron- and nickel-base alloys were etched electrolytically using either (1) 10 wt % oxalic acid in water, or (2) 32 vol % H_3PO_4 (concentrated, commercial), 59 vol % diethoxyethanol, and 9 vol % water. Because of the differences between the mounted specimens with respect to the contact

*Buehler, Ltd., Evanston, Illinois.

between the pellets and the molybdenum holder, the voltage and time required for etching varied substantially. In general, most specimens etched electrolytically at 6-25 V in 20 sec to 3 min. The vanadium-base alloys were chemically etched with a solution of 5 wt % $AgNO_3$ plus 2 vol % HF in water.

V. RESULTS AND DISCUSSION

A. Types 304 and 316 Stainless Steel

Tests for 4000 hr at 800°C indicated that carbon was transferred from stoichiometric or hyperstoichiometric (U,Pu)C to Type 304 stainless steel, but that the amount was relatively small. Metallographic evidence of carbon transfer was provided by the observation of heavier carbide precipitation along slip lines and the absence of sigma phase in the region adjacent to the fuel pellet, as shown in Fig. 3.* The slip lines apparently formed when the cladding was slightly deformed at the beginning of the heat treatment because of the difference in thermal-expansion coefficients between the test specimens and the molybdenum frame in which they were held. No sigma formation was observed in Type 304 stainless steel after 1000 hr at 800°C, but after 4000 hr, sigma was precipitated uniformly throughout the specimen, except within 280 μ of the interface with both stoichiometric and hyperstoichiometric (U,Pu)C. The composition of the Type 304 stainless steel used in these tests (18.6 wt % Cr, 8.8 wt % Ni, 0.69 wt % Si, 0.05 wt % C) lies in the gamma plus sigma phase field very near the gamma/(gamma + sigma) phase boundary.[1] The higher carbon content of the austenitic matrix, even though decreased by $M_{23}C_6$ precipitates, appears to be sufficiently high to prevent the formation of sigma phase near the interface.

The only other effect observed in both Types 304 and 316 stainless steel after the 800° tests was a small zone of 15-30 μ at the fuel-cladding interface that did not show the characteristic structure or slip lines found in the bulk of the specimen. The band was most clearly defined after the 1000-hr test, as is shown in Fig. 4. Electron-microprobe analyses revealed the iron content of the matrix of the band was about 3 wt % higher and the chromium content about 3 wt % lower than that of the unaffected steel. The nickel content was unchanged. A number of small precipitates consisting of approximately equal percentages of iron and chromium were found in the band and were believed to be carbides.

A test of Type 304 stainless steel and stoichiometric (U,Pu)C, at 1100°C for 400 hr, showed penetration of the steel, generally along grain boundaries, to a maximum depth of 135 μ. Electron-microprobe analysis revealed that the affected grain boundaries shown in Fig. 5, contained particles

*In Figs. 3-29, the cladding is shown at the top of the photomicrograph.

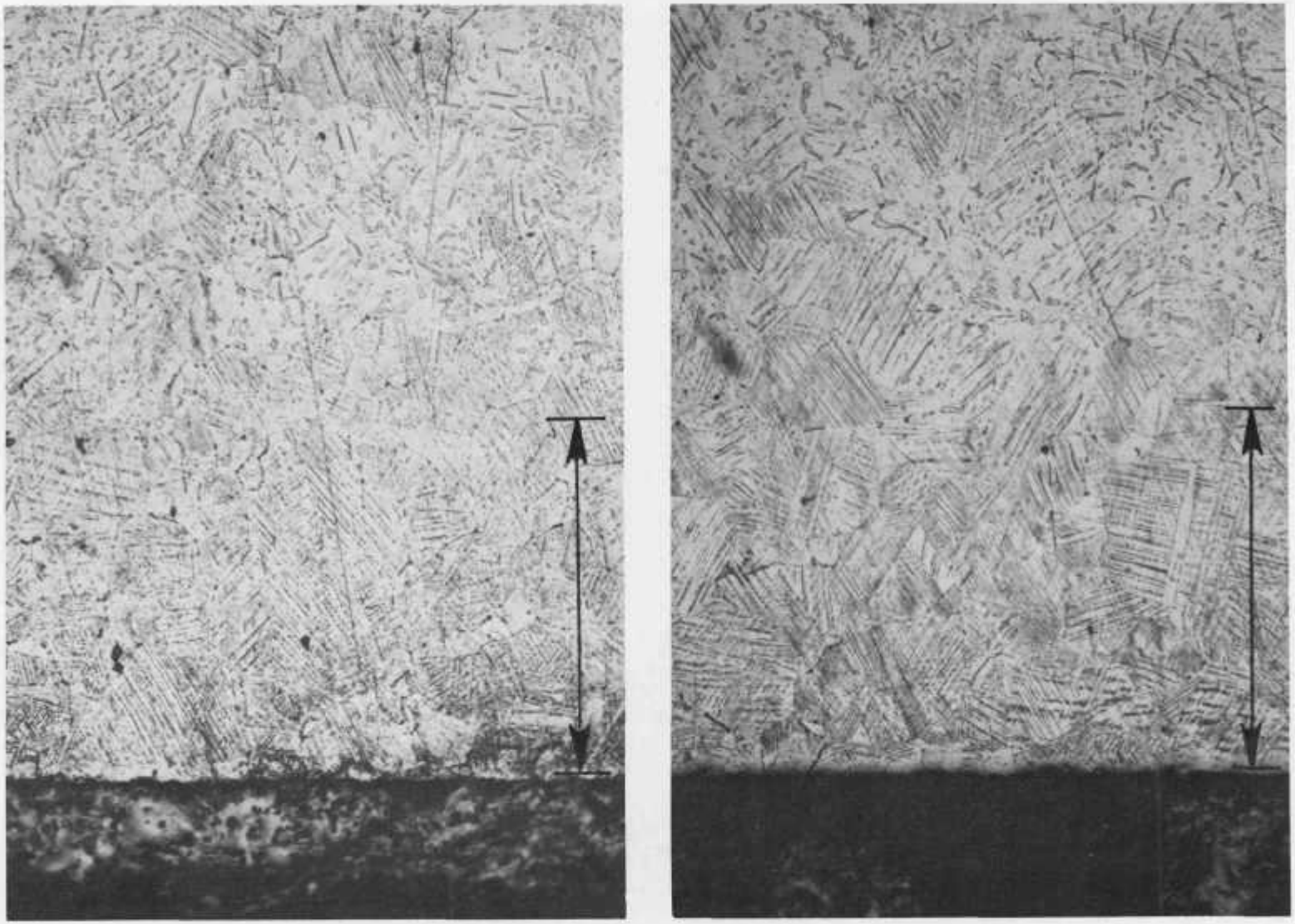

(a) Stoichiometric (U,Pu)C

(b) Hyperstoichiometric (U,Pu)C

Fig. 3. Type 304 Stainless Steel vs Stoichiometric and Hyperstoichiometric (U,Pu)C after 800°C Tests for 4000 hr. Zones with no sigma-phase formation are indicated by arrows. Mag. 200X. Neg. Nos. MSD-46270 and MSD-46273.

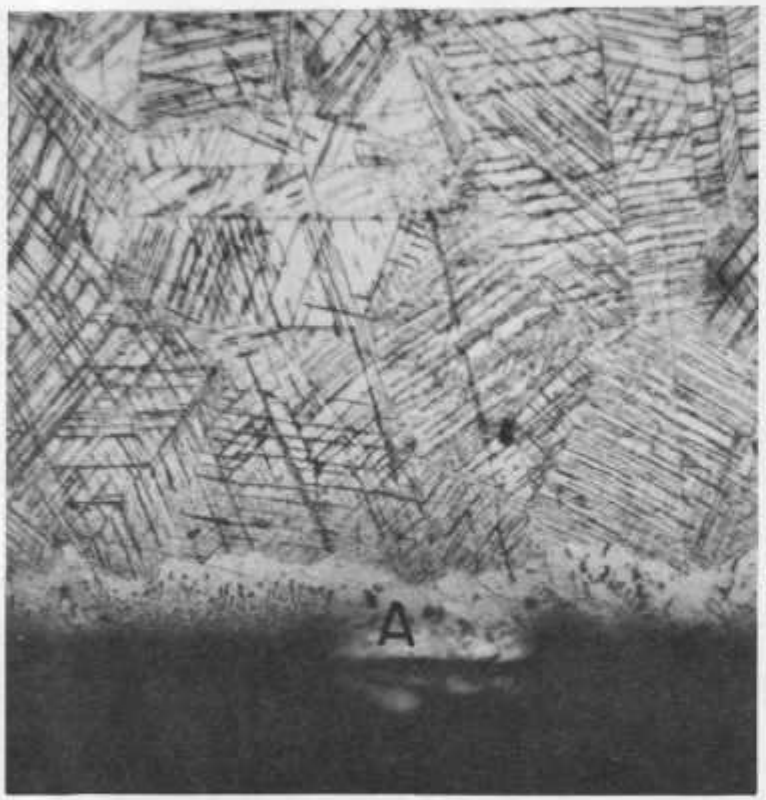

Fig. 4. Type 304 Stainless Steel vs Hyperstoichiometric (U,Pu)C after 800°C Tests for 1000 hr. A indicates the zone with carbide precipitates in the cladding but no slip lines. Mag. 500X. Neg. No. MSD-43576.

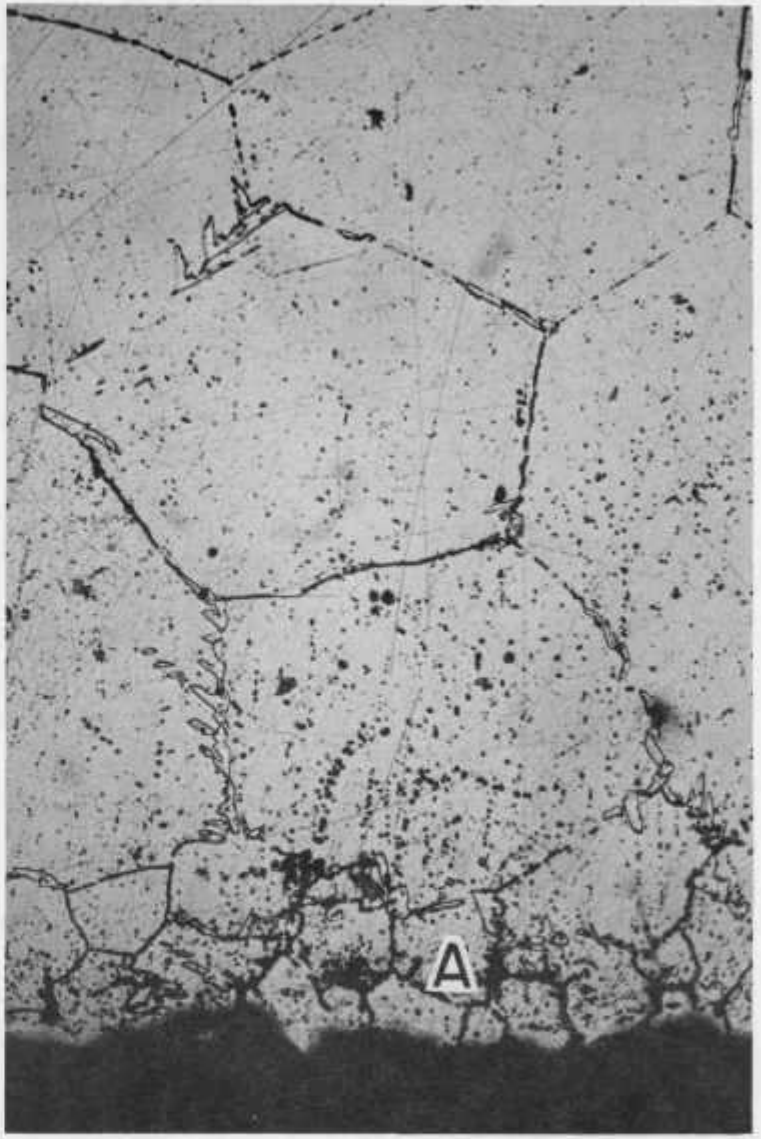

Fig. 5. Type 304 Stainless Steel vs (U,Pu)C after 1100°C Test for 400 hr. A indicates the area in which particles of high uranium and plutonium content were found. Mag. 500X. Neg. No. MSD-41130.

of relatively high uranium and plutonium content. In a 1000-hr test at this temperature, severe melting of the specimen occurred. The concentration of uranium and plutonium in the steel for the 400-hr test could reasonably have produced a eutectic in this quite complex system, which could have caused the melting found in the 1000-hr test. Eutectics in the binary systems Fe/U, Fe/Pu, Ni/U, and Ni/Pu are found at 1080, 1180, 1110, and 1220°C, respectively.[2]

Metallography revealed the same general results with Type 316 stainless steel as was found with Type 304. After the 1000-hr tests with stoichiometric and hyperstoichiometric (U,Pu)C, Type 316 stainless steel showed increased carbide precipitation within 200 μ of the interface and uniformly precipitated signa and possibly chi phases beyond this zone, as shown in Fig. 6. After 4000 hr, the intermetallic phases (sigma and chi) were found within 110 μ of the interface. The observation of the intermetallic phases nearer the interface after 4000 hr may be explained by the formation of a sigma phase from $M_{23}C_6$, or the longer time required for a sigma phase to precipitate in a high-carbon austenite matrix.

The mechanism for the slight carburization of stainless steels that was observed after compatibility tests with (U,Pu)C compositions of various carbon contents is not readily apparent. The transfer of carbon by gas phases (CO and/or CH_4) formed by the reaction of (U,Pu)C with impurities (O_2 and H_2O) introduced during fabrication of the carbide pellets was offered as an explanation,[3] but later findings did not substantiate this hypothesis.[4,5] Some carburization has been attributed to surface cold work brought about by machining the stainless steel specimens.[5] Surface oxidation of the carbide pellet specimens before assembly of the compatibility couples has also been reported as a possible cause of the subsequent carburization.[5]

In hyperstoichiometric (U,Pu)C, the presence of $(U,Pu)_2C_3$ offers a seemingly obvious source of carbon, but neither this investigation nor others have produced any conclusive evidence that a chemical reduction of $(U,Pu)_2C_3$ particles near the fuel-cladding interface has occurred. To determine directly the interaction of $(U,Pu)_2C_3$ with Types 304 and 316 stainless steel, compatibility tests with the $(U,Pu)_2C_3$ composition were run for 1000 hr at 800°C. In both cases, the $(U,Pu)_2C_3$ in contact with stainless steel was affected to a depth of 5-7 μ, as shown in Fig. 7. Electrolytic etching of the fuel indicated that this reaction was not a layer of (U,Pu)C formed by the reduction of $(U,Pu)_2C_3$. The composition of this layer was not identified, but its small size indicates that the interaction of stainless steel with $(U,Pu)_2C_3$ particles in a monocarbide matrix would be of little technological consequence.

B. 16-25-6 and 16-15-6 Alloys

The 16-25-6 and 16-15-6 alloys behaved similarly with both stoichiometric and hyperstoichiometric (U,Pu)C. The results of the metallographic observations are given in Table V. Figure 8 is a typical photomicrograph

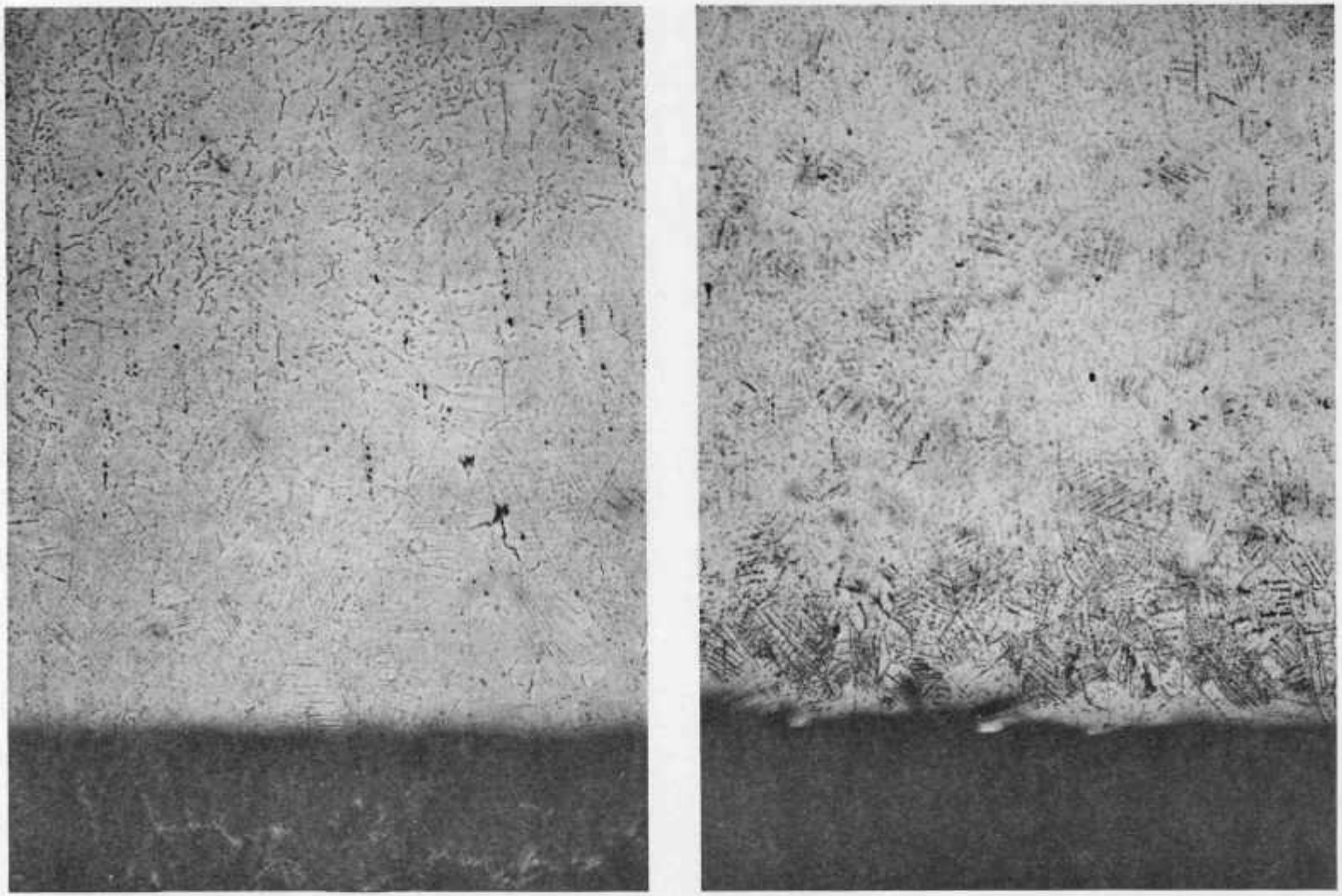

(a) 1000 hr

(b) 4000 hr

Fig. 6. Type 316 Stainless Steel vs Hyperstoichiometric (U,Pu)C after 800°C Test for 1000 and 4000 hr. Mag. 200X. Neg. Nos. MSD-49783 and MSD-48968.

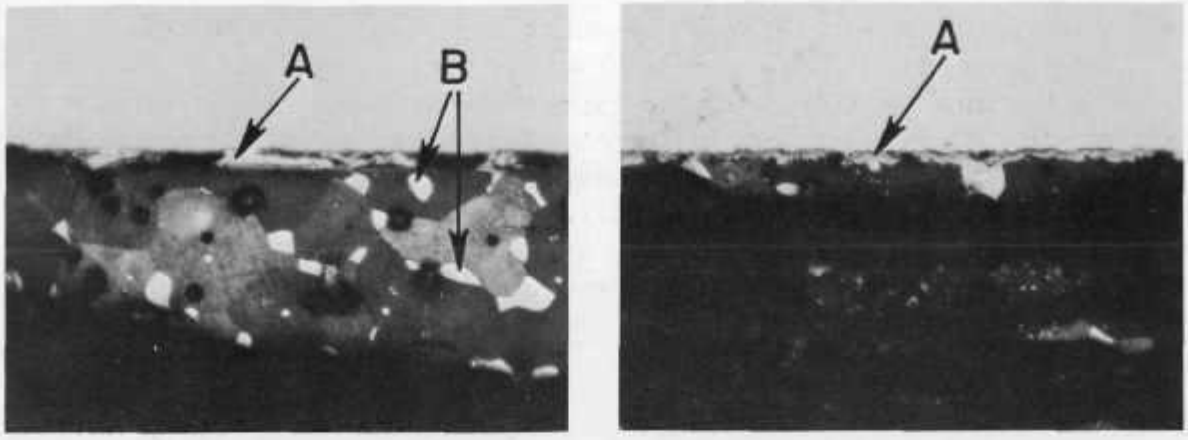

(a) Type 304 Stainless Steel (b) Type 316 Stainless Steel

Fig. 7. Types 304 and 316 Stainless Steel vs $(U,Pu)_2C_3$ after 800°C Tests for 1000 hr Showing Small Unidentified Reaction Product A at the Interface. Phase B is (U,Pu)C impurity. Mag. 375X. Neg. Nos. MSD-47494 and MSD-47496.

TABLE V. Depth of Precipitates Observed Metallographically in Iron-base Alloys after Contact with (U,Pu) Carbides

Alloy	Temperature, °C	Time, hr	Stoichiometric (U,Pu)C, 4.83 wt % equivalent C		Hyperstoichiometric (U,Pu)C, 5.25 wt % equivalent C		Hypostoichiometric $(U,Pu)_2C_3$, 6.90 wt % equivalent C	
			Average, μ	Maximum, μ	Average, μ	Maximum, μ	Average, μ	Maximum, μ
16-15-6	800	1000	28	34	35	38	-	-
16-25-6	800	1000	26	30	32	36	30	35
	800	4000	-	-	28	32	-	-
Haynes 56	800	1000	Nil	-	Nil	-	-	-
	-	4000	-	-	Nil	-	-	-

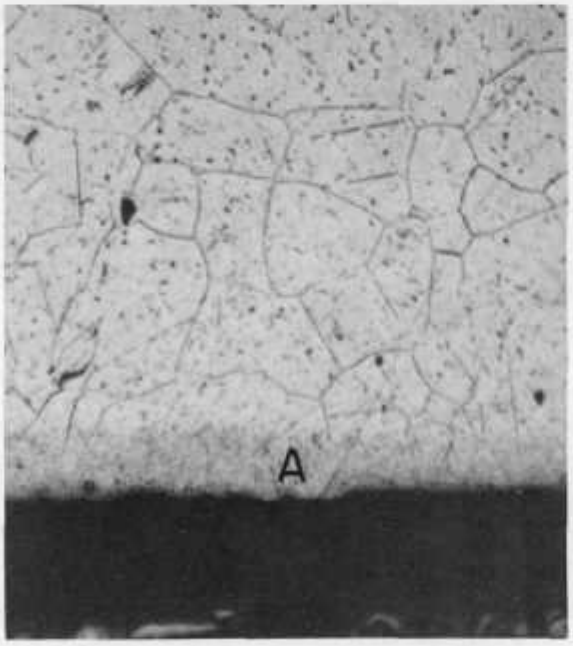

Fig. 8

Timken Alloy 16-25-6 vs (U,Pu)C after 800°C Test for 1000 hr. A indicates the zone of fine precipitates in the cladding at the interface. Mag. 375X. Neg. No. MSD-43573.

that shows the effect on these alloys after heat treatment at 800°C in contact with stoichiometric (U,Pu)C for 1000 hr. Although the affected zone in the alloy was somewhat larger for the hyperstoichiometric composition (containing ~20% $(U,Pu)_2C_3$) than for the stoichiometric composition, no additional increase was evident for the composition containing ~90% $(U,Pu)_2C_3$. A test of 16-25-6 alloy and hyperstoichiometric $(U,Pu)_2C_3$ at 800°C for 4000 hr showed no increase in the depth of the affected zone over that found at 1000 hr. Although the testing was limited, the results indicate that the depth of precipitation in these alloys was not directly related to either time or carbon content of the (U,Pu) carbide compositions.

The affected zones of these alloys, when etched, appeared to contain a large number of very small precipitates. An electron-microprobe study of a specimen containing 16-25-6 alloy heat-treated for 1000 hr at 800°C indicated that, among the major elements in the alloy, the distribution of molybdenum had been most significantly affected. The matrix of the unaffected material was found to contain about 3.5 wt % molybdenum, whereas the grain boundaries and spots within grains, although small in size, registered peaks indicating 14-19 wt % molybdenum. The fine particles in the affected zone, believed to be molybdenum-rich, were too small for even semiquantitative results. A traverse across the affected zone using a beam size of 1-2 μ showed relatively small variations in molybdenum content of 5-7 wt %.

C. Haynes 56

Although Haynes 56 is no longer produced commercially, it is a good example of an iron-base alloy that is significantly stronger than Types 304 or 316 stainless steel and is unaffected by prolonged contact with hyperstoichiometric (U,Pu)C. No compatibility effects were found after testing this alloy at 800°C with the stoichiometric and hyperstoichiometric (U,Pu)C for 1000 and 4000 hr. Likewise, no effect was observed in tests of this material with the $(U,Pu)_2C_3$ composition after 1000 hr at 800°C or with the stoichiometric and hyperstoichiometric (U,Pu)C after 1000 hr at 900°C. A typical microstructure of this material after an 800°C compatibility test is shown in Fig. 9.

D. Inconel 625

Inconel 625 contained the highest nickel content (61 wt %) of the alloys tested and was found to be the least compatible with carbide fuels. Three distinct zones were formed after 1000-hr tests with the stoichiometric and hyperstoichiometric (U,Pu)C compositions. As shown in Figs. 10 and 11, two zones were in the cladding and one was in the fuel. The sizes of these zones after heat treatments at 700 and 800°C are compared in Table VI. The reaction zones found in the 800°C compatibility test specimen containing hyperstoichiometric (U,Pu)C were analyzed by means of an electron microprobe. The reaction zone in the fuel has been identified as $(U,Pu)Ni_5$. This

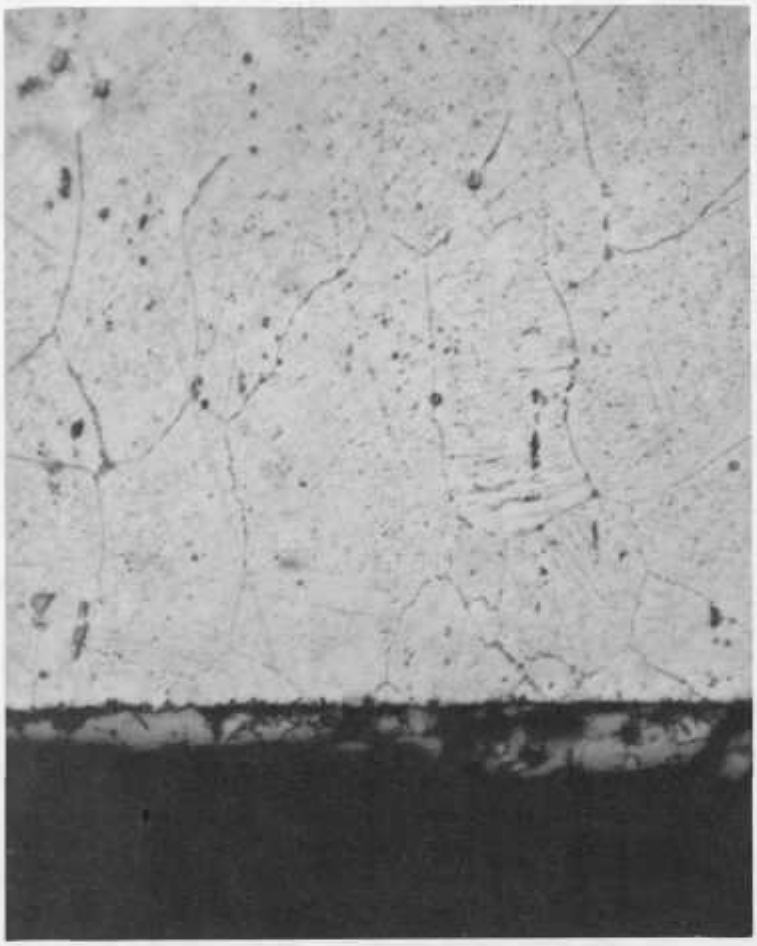

Fig. 9

Haynes 56 vs Hyperstoichiometric (U,Pu)C after 800°C Test for 4000 hr. No effects on the cladding were observed. Mag. 500X. Neg. No. MSD-44025.

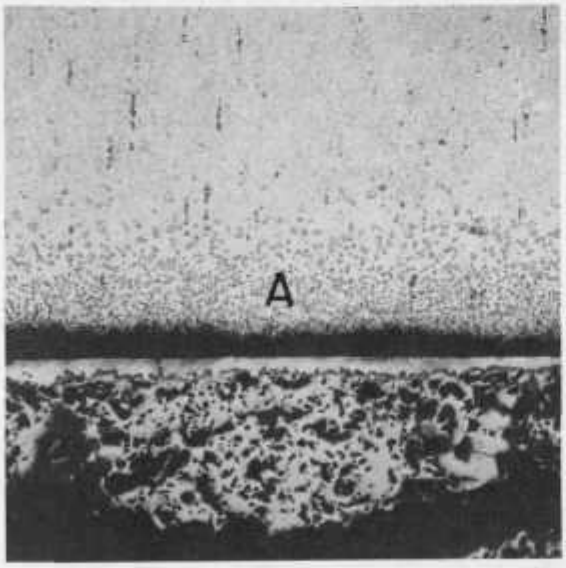

(a) 150X

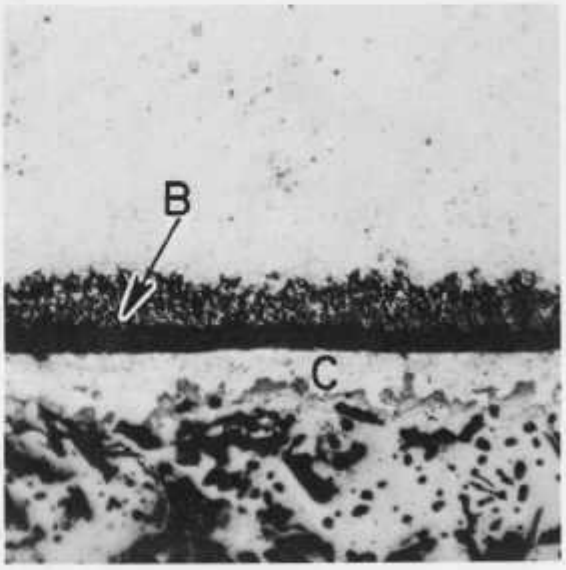

(b) 375X

Fig. 10. Inconel 625 vs (U,Pu)C after 800°C Test for 1000 hr. A is the precipitate zone in the cladding, B is the mottled chromium- and molybdenum-rich zone in the cladding, and C is the $(U,Pu)Ni_5$ zone in the fuel. Neg. Nos. MSD-45378 and MSD-45379.

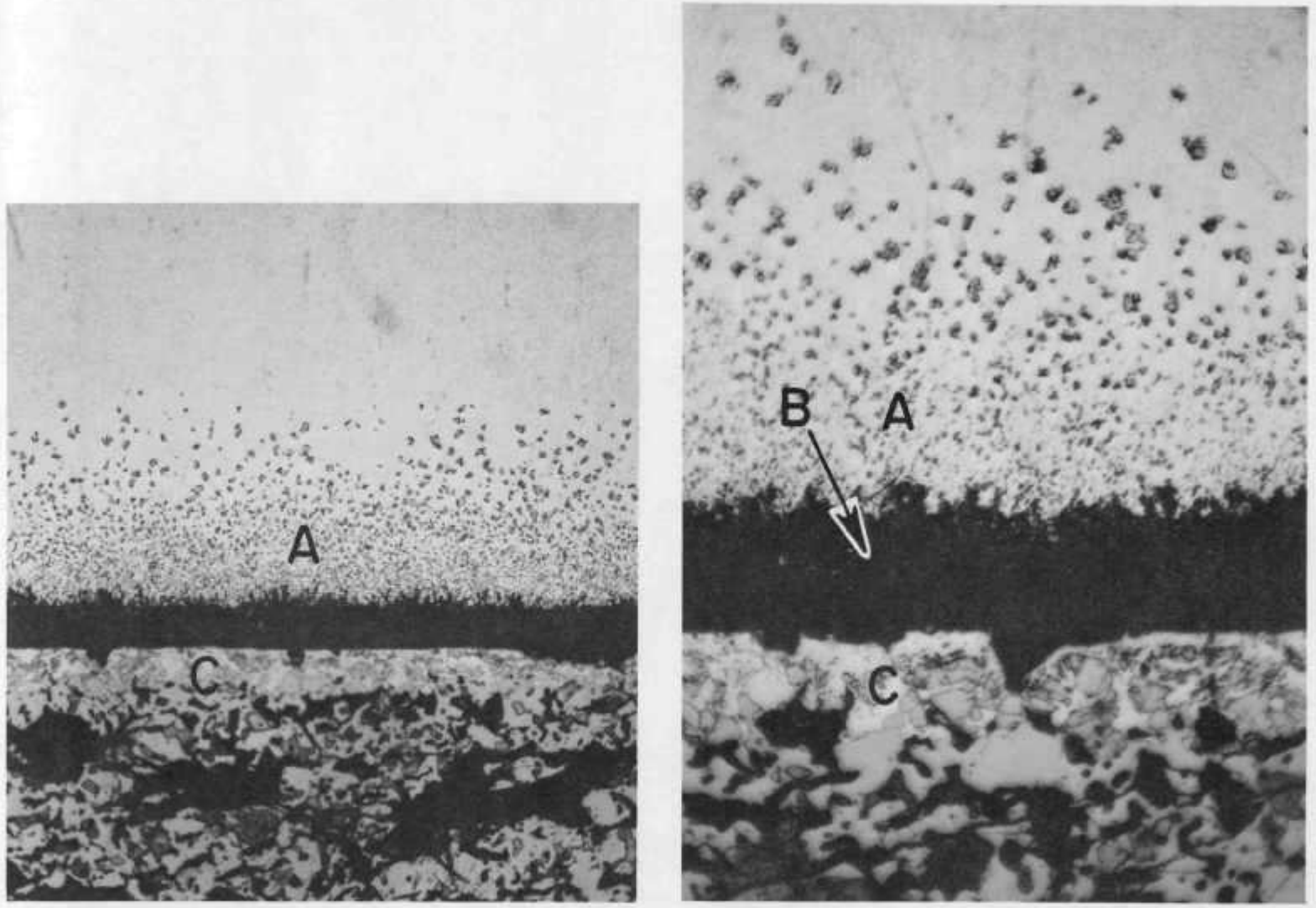

(a) 200X (b) 500X

Fig. 11. Inconel 625 vs Hyperstoichiometric (U,Pu)C after 800°C Test for 1000 hr. A is the precipitate zone in the cladding, B is the mottled chromium- and molybdenum-rich zone in the cladding, and C is the (U,Pu)Ni_5 zone in the fuel. Neg. Nos. MSD-45386 and MSD-45387.

TABLE VI. Extent of Zones Observed Metallographically in Three Commercial Nickel-base Alloys after Contact with (U,Pu) Carbides for 1000 hr

Alloy	Temperature, °C	Carbide Composition, wt % equivalent carbon	Thickness of U-Pu-Ni Zone in Fuel, μ		Thickness of Cr-rich Zone in Cladding, μ		Precipitate Depth from Interface, μ	
			Average	Maximum	Average	Maximum	Average	Maximum
Incoloy 800	700	4.83	3	5	4	6	Nil	-
Incoloy 800	800	4.83	5	8	4	6	125	160
		6.75	7	15	4	6	125	160
Hastelloy-X	700	4.83	Nil	-	Nil	-	Nil	-
		5.25	-	4	-	2	Nil	-
		6.75	2	4	2	2	Nil	-
Hastelloy-X	800	4.83	5	8	3	5	Nil	-
		5.25	-	8	-	7	Nil	-
		6.75	8	10	6	12	125	175
Inconel 625	700	4.83	18	30	20	25	45	55
		5.25	18	30	20	25	45	55
		6.75	Nil	-	Nil	-	20	30
Inconel 625	800	4.83	25	37	23	30	130	160
		5.25	36	44	26	36	145	180
		6.75	7	10	Nil	-	65	80

compound could be expected in high-nickel alloys, since UNi_5 has been shown to be the principal product formed in a diffusion couple of uranium carbide versus nickel heat-treated at 800°C for 950 hr.[6] A continuous network of $(U,Pu)Ni_5$ surrounding (U,Pu)C grains was formed in the hyperstoichiometric (U,Pu)C, in contrast to the solid $(U,Pu)Ni_5$ band formed in the single-phase (U,Pu)C. Evidence that the (U,Pu)C grains within the $(U,Pu)Ni_5$ network were formed by reduction of the $(U,Pu)_2C_3$ grains in the initial material will be given later in this section.

The dark, mottled, small zone on the cladding side of the interface appeared to be composed of two bands of rather complex composition containing high percentages of chromium. The approximate compositions of these bands are given in Table VII. Percentages of carbon (5.25 wt % in the fuel) and niobium and tantalum (4 wt % in the cladding) were not determined. Although no uranium was found on the cladding side of the interface, up to 5 wt % plutonium was found in the mottled zone.

TABLE VII. Composition of Reaction Zones: Hyperstoichiometric (U,Pu)C vs Inconel 625 (800°C for 1000 hr)

Element	(U,Pu)C, wt %	Reaction Zones, wt %						Unaffected Inconel 625, wt %
		$(U,Pu)Ni_5$ Zone in Fuel (36-μ width), 36 μ	Mottled Reaction Zone in Cladding (26-μ width)		Precipitate Zone (120-μ width)			
			8 μ	18 μ	12 μ	Precip.	108 μ	
U	76	34	-	-	-	-	-	-
Pu	19	12	1	5	-	-	-	-
Ni	-	54	10	21	61	24	70 – 61	61
Cr	-	-	52	43	20	61	15 – 22	22
Mo	-	-	13	16	7	14	7 – 9	9
Fe	-	-	1	0.5	8	1	4 – 3	3

Beyond the mottled reaction zone in the cladding, a zone of chromium-rich precipitates was observed. In the area containing these precipitates, three observations were made: (1) A 12-μ band immediately adjacent to the mottled zone was richer in iron than any other portion of the cladding;

(2) nickel and iron contents continuously decreased throughout this area from the iron-enriched band to the unaffected cladding matrix, whereas the chromium and molybdenum contents continuously increased; and (3) the precipitates, which were numerous and small close to the original interface, became less frequent but larger as the distance from the interface increased.

Although the reaction of Inconel 625 with the hyperstoichiometric carbide composition containing 20% $(U,Pu)_2C_3$ was slightly greater than that with the single-phase (U,Pu)C, the total reaction depth with the $(U,Pu)_2C_3$ composition was significantly smaller. Only the precipitates were observed on the cladding side of the interface, the dark, mottled zone was absent, and less $(U,Pu)Ni_5$ was formed in the fuel. However, two other zones were observed on the fuel side of the interface, as shown in Fig. 12. Beyond the $(U,Pu)Ni_5$ zone, a 4-μ gray layer occurred, and beyond this, a 9-μ zone of monocarbide resulting from reduction of the sesquicarbide phase. The gray layer, found by microprobe analysis to have a high oxygen content, is probably $(U,Pu)O_2$. The cladding is believed to be the source of the oxygen, since no other surface of the fuel pellet exhibited any oxide formation. Evidence of oxygen diffusion into the fuel can also be seen in Fig. 10, where the gray phase is located between the $(U,Pu)Ni_5$ and the (U,Pu)C phases.

E. Hastelloy-X

Hastelloy-X was affected in a manner similar to that observed with Inconel 625. Because of the lower nickel content (47 wt %), however, the reaction zones were significantly smaller than those found with Inconel 625. The sizes of the reaction zones are listed in Table VI.

At 700°C, no reaction was observed between Hastelloy-X and (U,Pu)C (4.83 wt % C) for up to 4000 hr. Intermittent reaction with $(U,Pu)_2C_3$ along the interface was observed in the case of hyperstoichiometric (U,Pu)C (5.25 wt % C) at this temperature but, as shown in Fig. 13, no increase in the size of these small reaction areas was found after 4000 hr. A test with the $(U,Pu)_2C_3$ composition (6.75 wt % C) at 700°C for 1000 hr revealed a 4-μ reaction zone (equivalent to the maximum found with the hyperstoichiometric (U,Pu)C) and also an adjacent 8-μ zone in the fuel that had been reduced to (U,Pu)C, as shown in Fig. 14.

After 1000 hr at 800°C, both (U,Pu)C and hyperstoichiometric (U,Pu)C reacted with Hastelloy-X to form $(U,Pu)Ni_5$ and a chromium-rich zone in the cladding (see Fig. 15). Figure 15b illustrates the greater extent of the reaction at those points in contact with the $(U,Pu)_2C_3$ phase. After 4000 hr at 800°C, inter- and intragranular precipitation in Hastelloy-X was found to an average depth of 90 μ (maximum depth of 140 μ), as shown in Fig. 16. However, no increases in the average depth of the $(U,Pu)Ni_5$ layer or the chromium-rich layer were found after the longer heat treatment. Likewise, the larger reaction zones found in areas where the cladding was in contact with the $(U,Pu)_2C_3$ phase had not significantly increased.

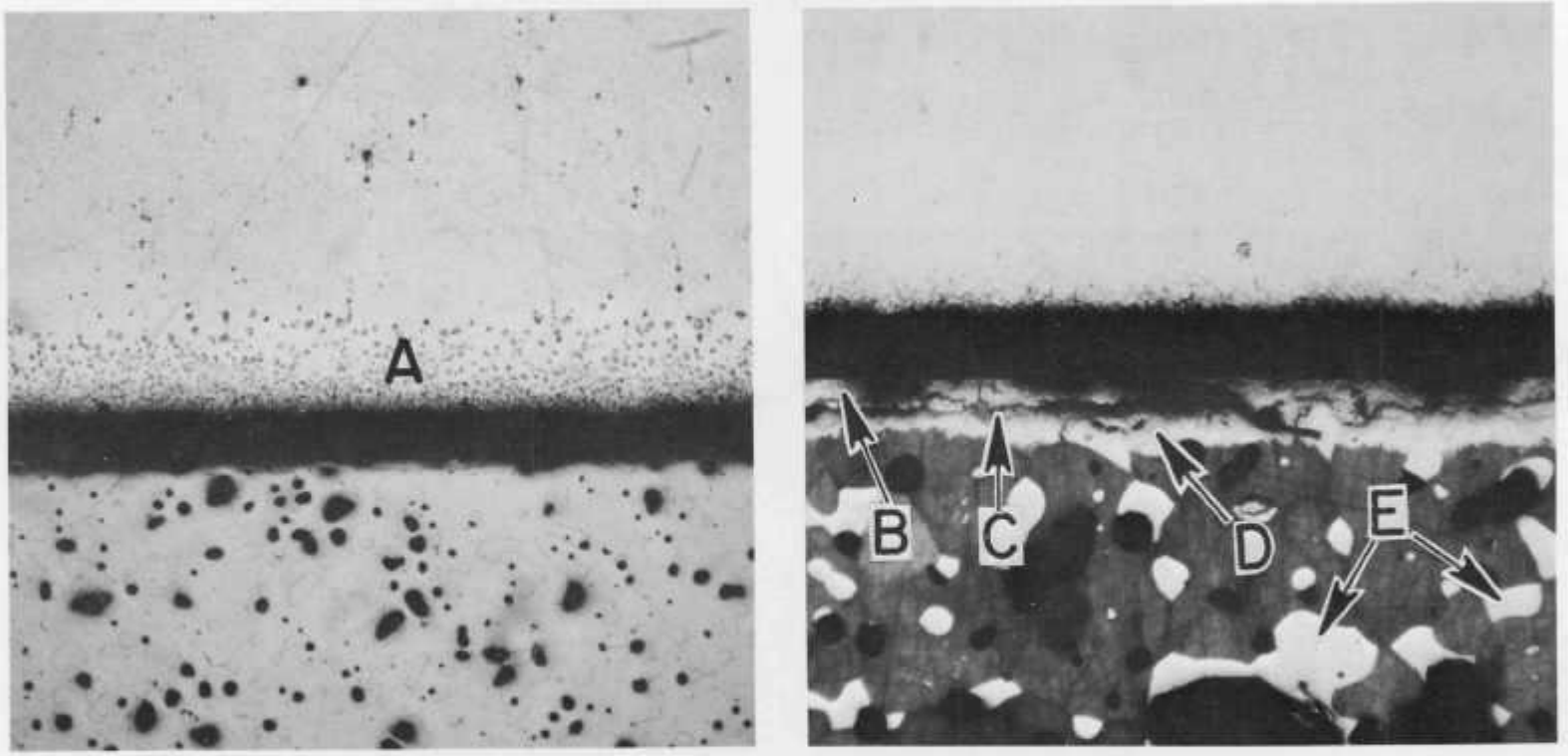

(a) 200X (b) 500X

Fig. 12. Inconel 625 vs $(U,Pu)_2C_3$ after 800°C Test for 1000 hr. A is the precipitate zone in the cladding, B is the $(U,Pu)Ni_5$ zone in the fuel, C is the gray (oxide) zone, D is the (U,Pu)C zone formed by reduction of $(U,Pu)_2C_3$, and E is the (U,Pu)C impurity. Neg. Nos. MSD-46715 and MSD-46713.

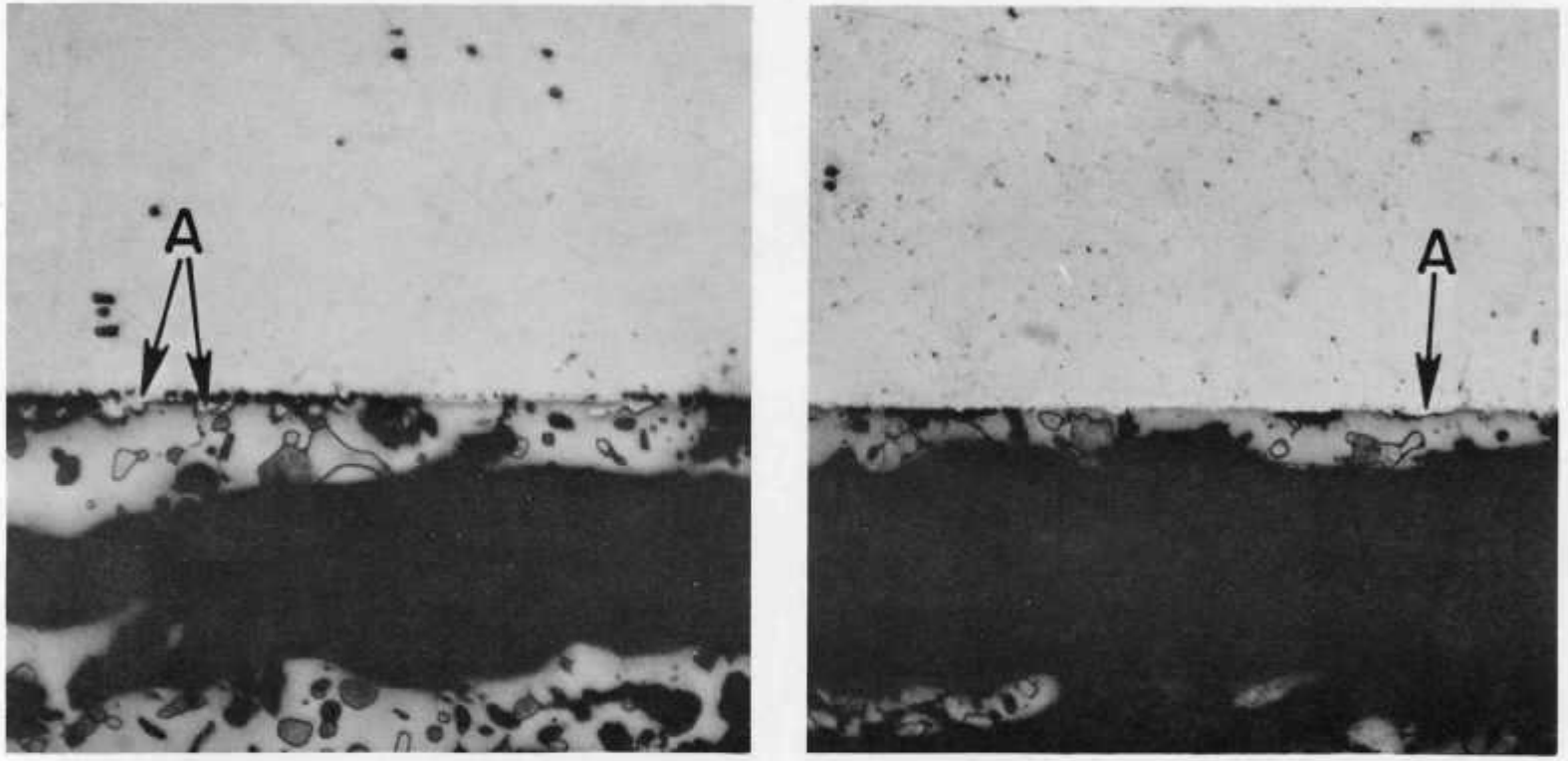

(a) 1000 hr

(b) 4000 hr

Fig. 13. Hastelloy-X vs Hyperstoichiometric (U,Pu)C after 700°C Tests for 1000 and 4000 hr. A indicates the reaction product formed by reaction of the cladding with $(U,Pu)_2C_3$ particles. Mag. 500X. Neg. Nos. MSD-44693 and MSD-46669.

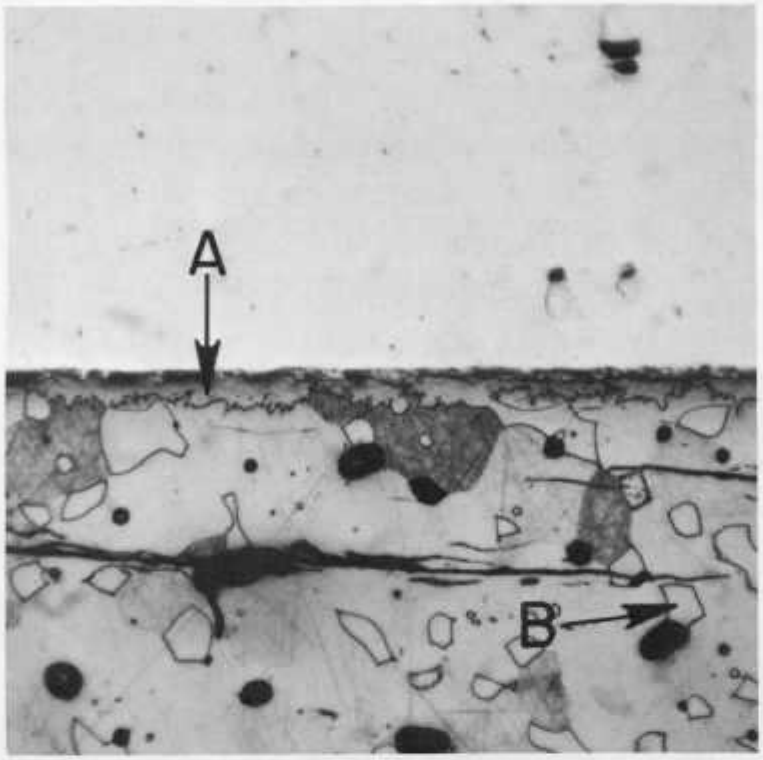

Fig. 14

Hastelloy-X vs $(U,Pu)_2C_3$ after 700°C Test for 1000 hr. A is the (U,Pu)C zone formed by reduction of $(U,Pu)_2C_3$, and B is the (U,Pu)C impurity. Mag. 500X. Neg. No. MSD-46673.

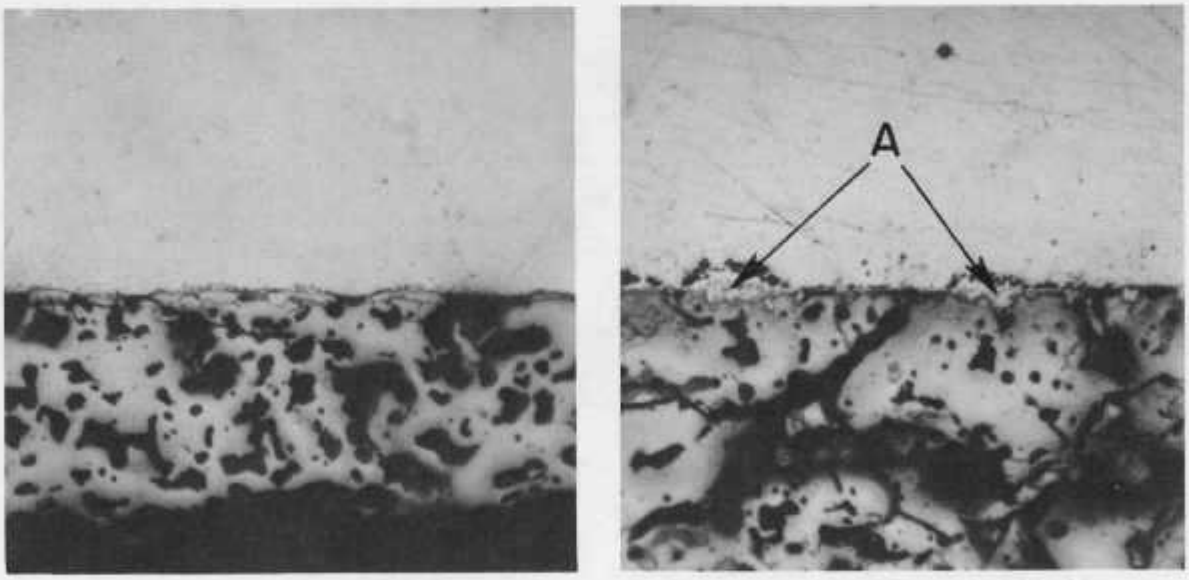

(a) Stoichiometric (U,Pu)C

(b) Hyperstoichiometric (U,Pu)C

Fig. 15. Hastelloy-X vs Stoichiometric and Hyperstoichiometric (U,Pu)C after 800°C Tests for 1000 hr. A indicates increased reaction at points of contact with $(U,Pu)_2C_3$ particles. Mag. 375X. Neg. Nos. MSD-41269 and MSD-43636.

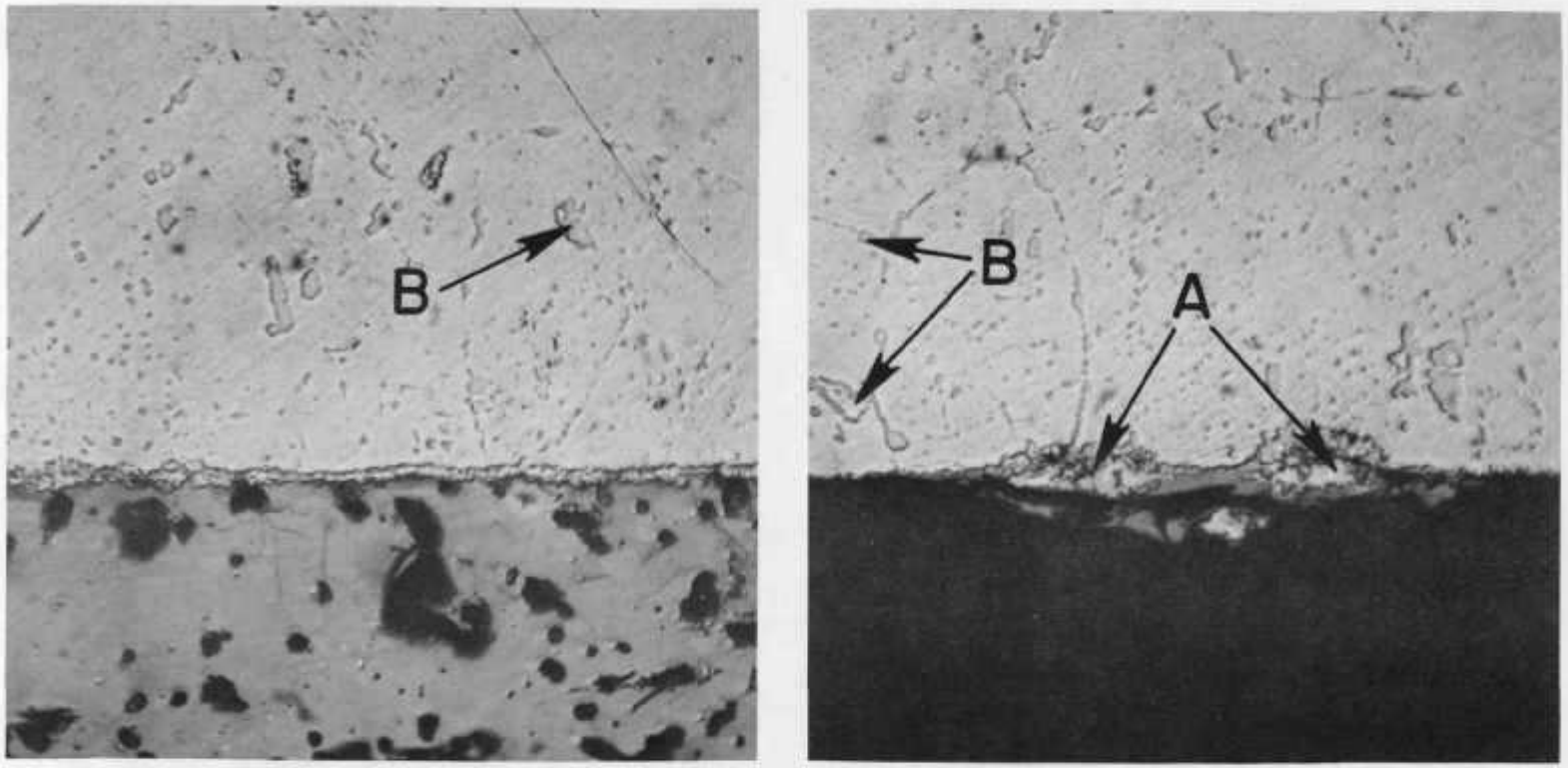

(a) Stoichiometric (U,Pu)C

(b) Hyperstoichiometric (U,Pu)C

Fig. 16. Hastelloy-X vs Stoichiometric and Hyperstoichiometric (U,Pu)C after 800°C Tests for 4000 hr. A indicates increased reaction at points of contact with $(U,Pu)_2C_3$ particles, and B the precipitates in cladding. Mag. 500X. Neg. Nos. MSD-49155 and MSD-49156.

The reaction with the $(U,Pu)_2C_3$ composition at 800°C revealed, in addition to the $(U,Pu)Ni_5$ zone, a gray layer of about 5 μ, which was believed to be $(U,Pu)O_2$, and a 25-μ layer of (U,Pu)C that was the result of the reduction of $(U,Pu)_2C_3$. These results, shown in Fig. 17, are similar to those obtained with Inconel 625.

F. Incoloy 800

Although the nickel content of Incoloy 800 is significantly less than that of Hastelloy-X, the formation of an intermetallic phase in the fuel occurred to the same depth with either alloy after contact with (U,Pu)C for 1000 hr at 800°C. With Incoloy 800, however, the intermetallic phase, shown in Fig. 16, contained approximately equal atomic percentages of nickel and iron and about 25 at. % (U + Pu). The chromium- and molybdenum-rich zones found in the compatibility tests with Inconel 625 and Hastelloy-X were not found in Incoloy 800, which contains no molybdenum. However, extensive, fine, chromium-rich inter- and intragrain carbide precipitates were found in Incoloy 800 after contact with (U,Pu)C or $(U,Pu)_2C_3$ at 800°C, as shown in Figs. 18b and 19b. The sizes of the reaction zones for the tests on Incoloy 800 are listed in Table VI.

In the test with the $(U,Pu)_2C_3$ composition, reduction of $(U,Pu)_2C_3$ to (U,Pu)C occurred to an average depth of 24 μ from the fuel-cladding interface. Formation of the gray phase was observed in the fuel to an average depth of 14 μ, as shown in Fig. 19a.

G. Vanadium Alloys

Of the several vanadium-base alloys developed as cladding for nuclear fuels, seven were tested with (U,Pu) carbide fuels. Four were developed at ANL and designated by nominal composition: V-20 wt % Ti, V-15 wt % Ti-7.5 wt % Cr, V-15 wt % Cr-5 wt % Ti, and V-10 wt % Cr. Three others were developed at Westinghouse Electric Corporation and designated as VANSTAR-7, VANSTAR-8, and VANSTAR-9. Chemical analyses of these alloys are given in Table II.

In the 700-800°C range, V-20 wt % Ti and V-15 wt % Ti-7.5 wt % Cr were carburized by (U,Pu)C. Photomicrographs of this effect are shown in Figs. 20 and 21. Chemical analyses of the carburized zone in the V-15 wt % Ti-7.5 wt % Cr specimen heat treated at 800°C for 1000 hr showed a carbon content of 0.9 wt %. At 800°C these alloys were able to reduce $(U,Pu)_2C_3$ to (U,Pu)C. Figure 22 shows a 38-μ zone of the $(U,Pu)_2C_3$ composition that was reduced to (U,Pu)C after contact with V-15 wt % Ti-7.5 wt % Cr for 1000 hr at 800°C. The depth of carburization (64 μ) of this alloy was essentially equal to that of the (U,Pu)C tests (see Fig. 21).

At 950°C, the formation of a carbide phase in V-20 wt % Ti was evident after 7 days (168 hr), and the reduction of (U,Pu)C to U + Pu metal was observed at (U,Pu)C grain boundaries, as shown in Fig. 23.

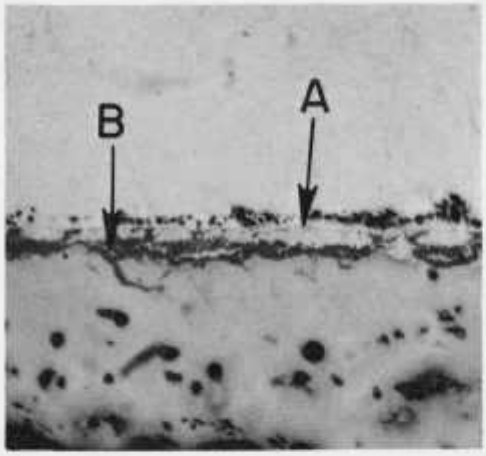

(a) As Polished

(b) Fuel Etched

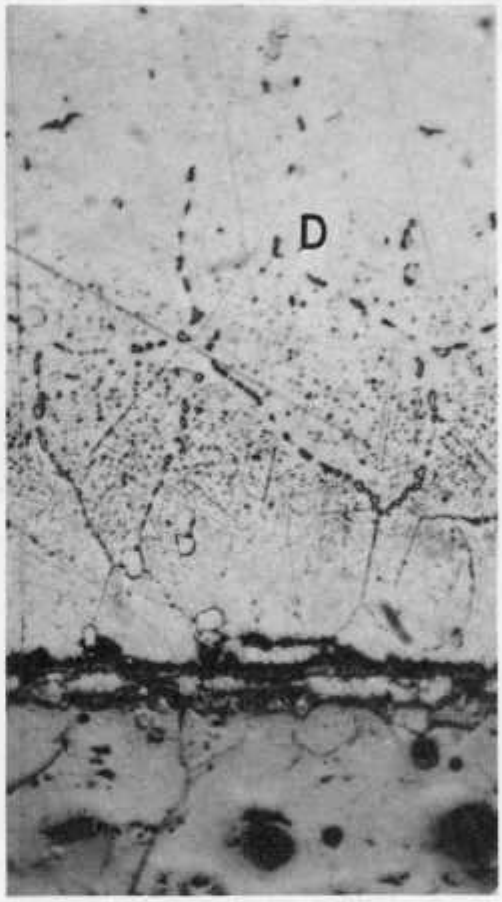

(c) Cladding Etched

Fig. 17. Hastelloy-X vs $(U,Pu)_2C_3$ after 800°C Test for 1000 hr. A is the $(U,Pu)Ni_5$ zone, B is the gray (oxide) zone, C is the (U,Pu)C zone formed by reduction of $(U,Pu)_2C_3$, and D is the precipitate zone in the cladding. Mag. 375X. Neg. Nos. MSD-46280, MSD-46674, and MSD-46279.

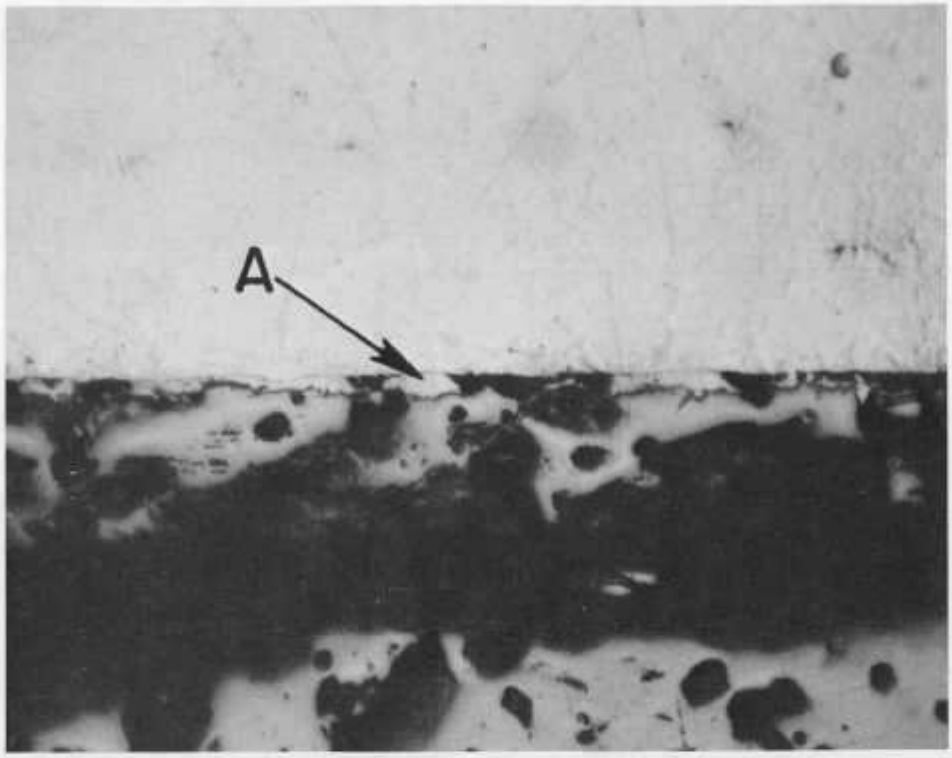

(a) 500X

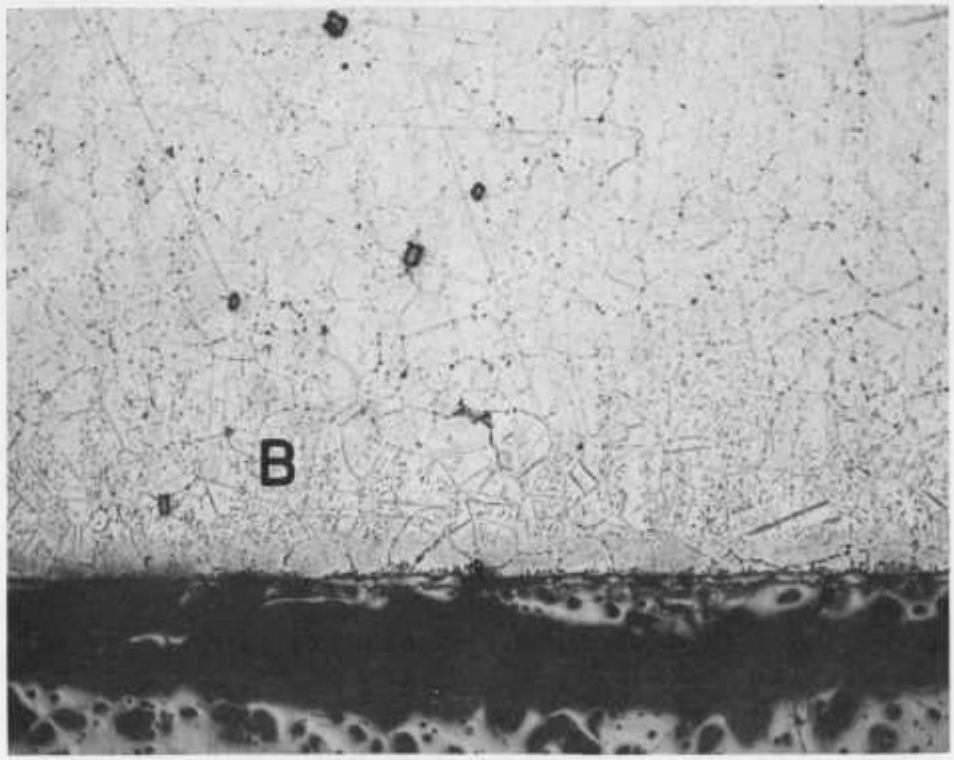

(b) 200X

Fig. 18. Incoloy 800 vs (U,Pu)C after 800°C Test for 1000 hr. A is the U-Pu-Ni-Fe phase in the fuel, and B is the precipitation zone in the cladding. Neg. Nos. MSD-47617 and MSD-47618.

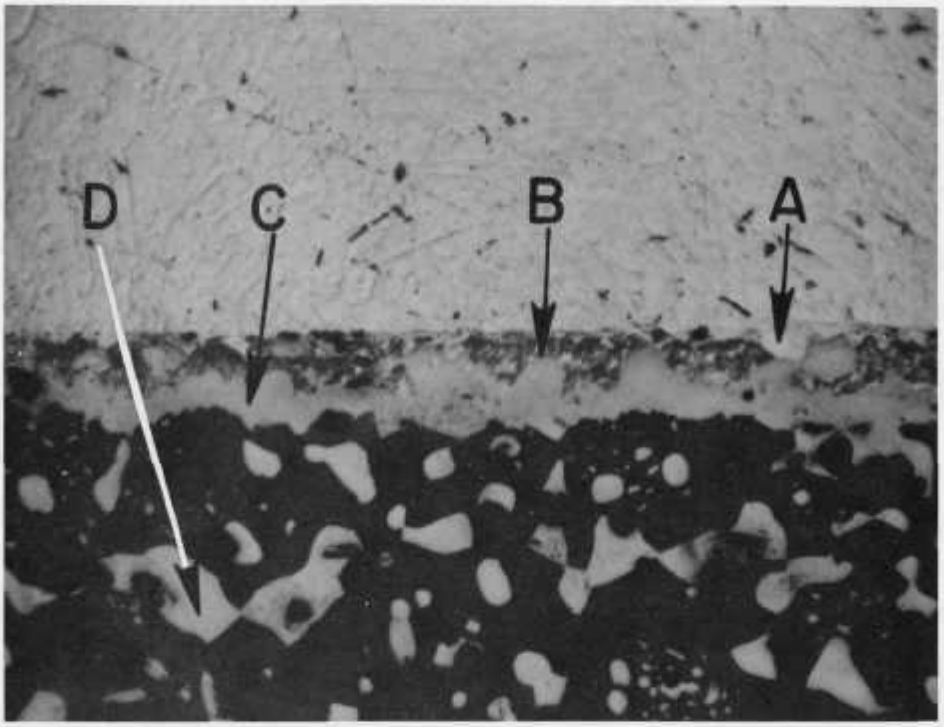

(a) 500X

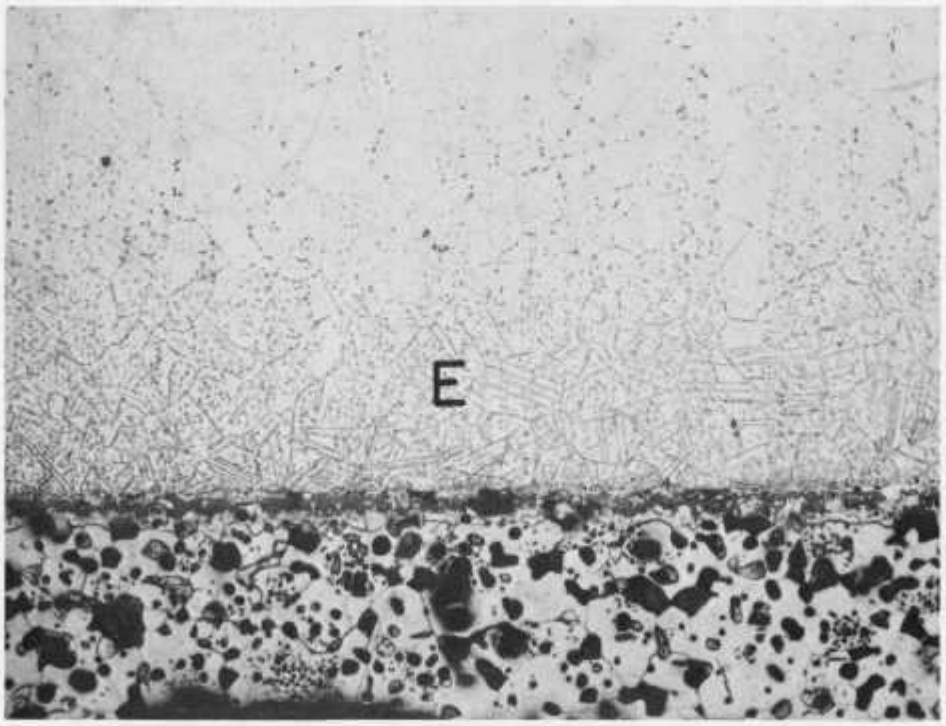

(b) 200X

Fig. 19. Incoloy 800 vs $(U,Pu)_2C_3$ after 800°C Test for 1000 hr. A is the U-Pu-Ni-Fe phase in the fuel, B is the gray (oxide) phase, C is the (U,Pu)C zone formed by reduction of $(U,Pu)_2C_3$, D is the (U,Pu)C impurity, and E is the precipitate zone in cladding. Neg. Nos. MSD-47500 and MSD-47502.

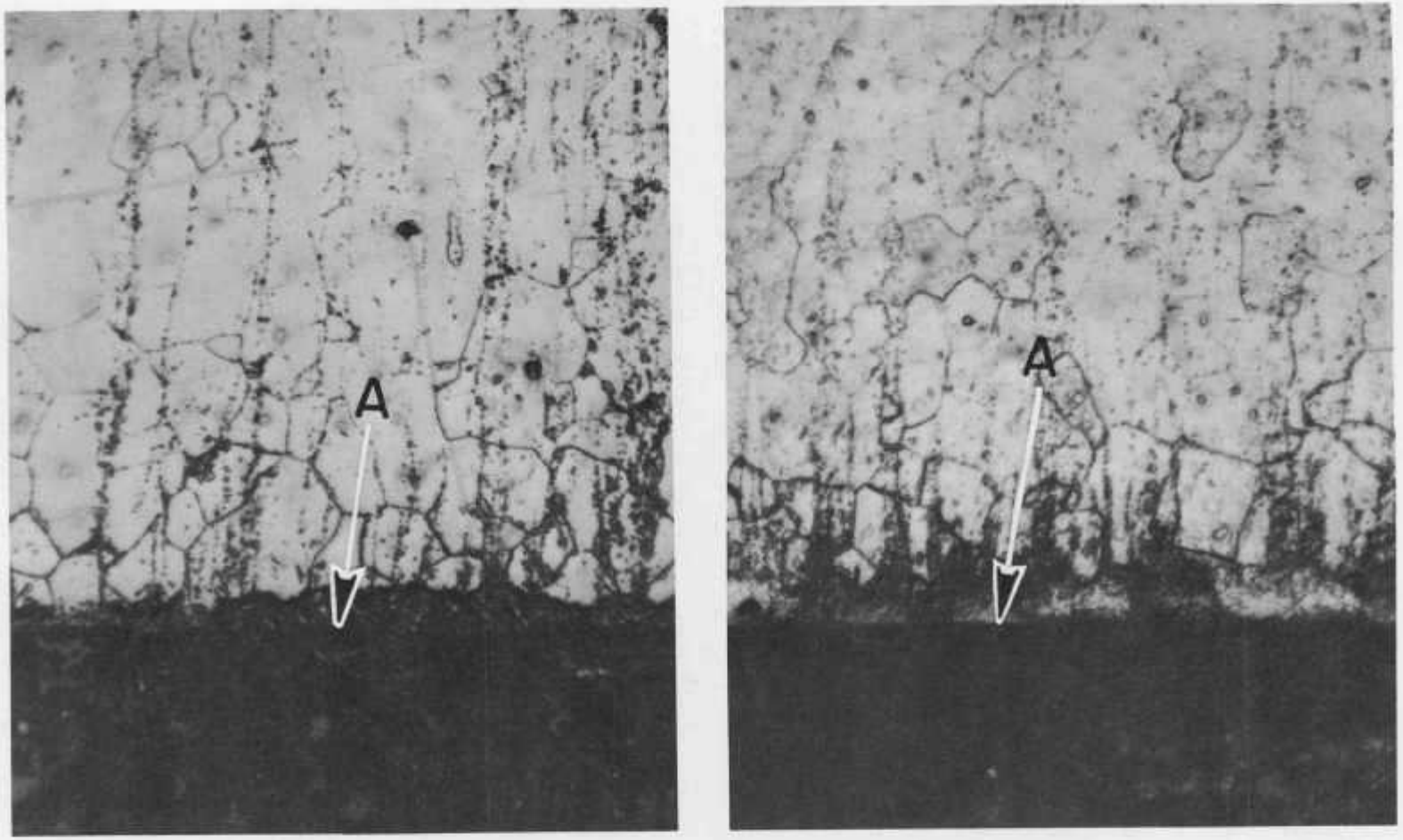

(a) Stoichiometric (U,Pu)C

(b) Hyperstoichiometric (U,Pu)C

Fig. 20. V-20 wt % Ti vs Stoichiometric and Hyperstoichiometric (U,Pu)C after 700°C Tests for 1000 hr. A is the carburized zone in the cladding. Mag. 500X. Neg. Nos. MSD-45932 and MSD-45933.

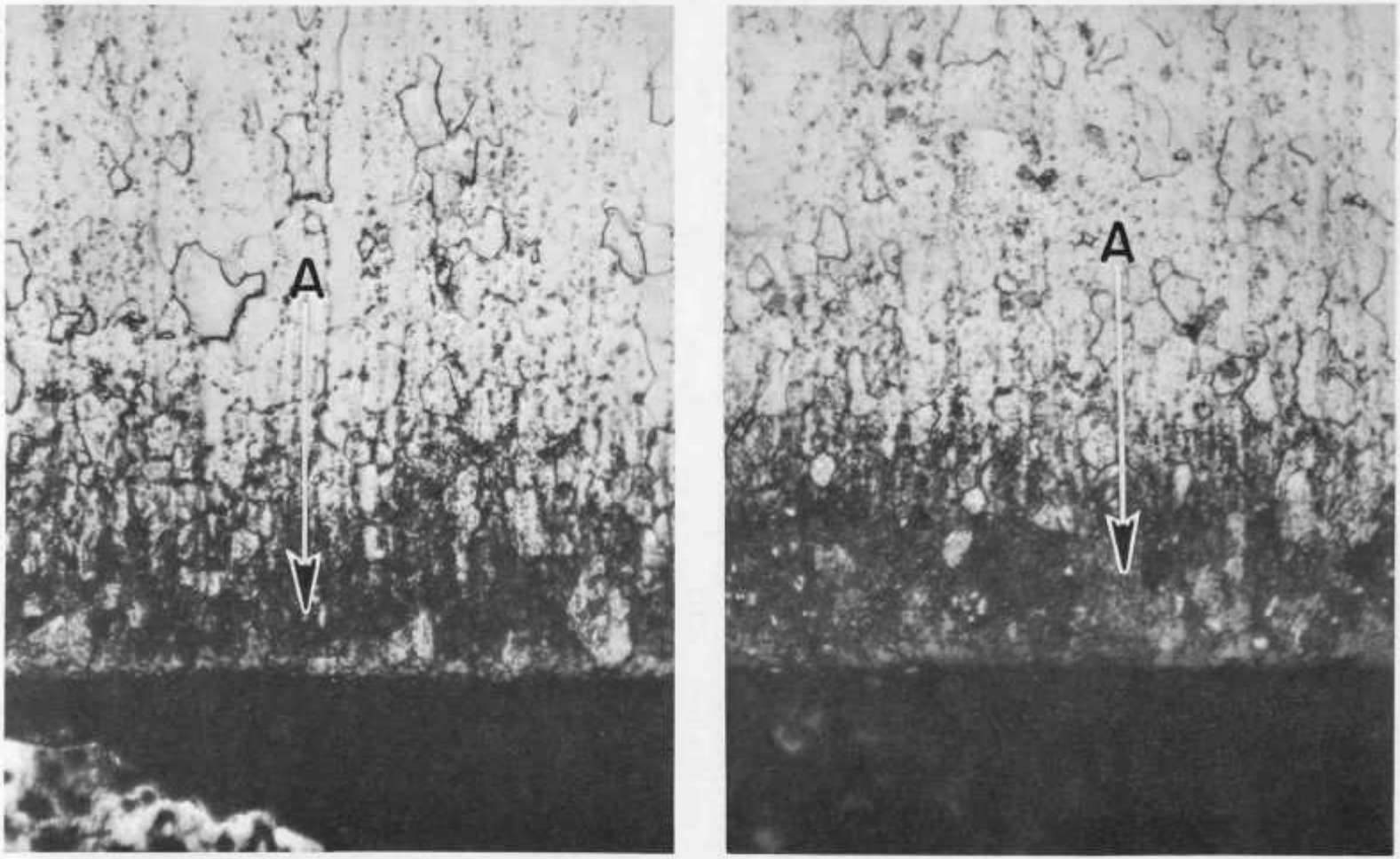

(a) Stoichiometric (U,Pu)C

(b) Hyperstoichiometric (U,Pu)C

Fig. 21. V–15 wt % Ti–7.5 wt % Cr vs Stoichiometric and Hyperstoichiometric (U,Pu)C after 800°C Tests for 1000 hr. A is the carburized zone in the cladding. Mag. 500X. Neg. Nos. MSD–47313 and MSD–47314.

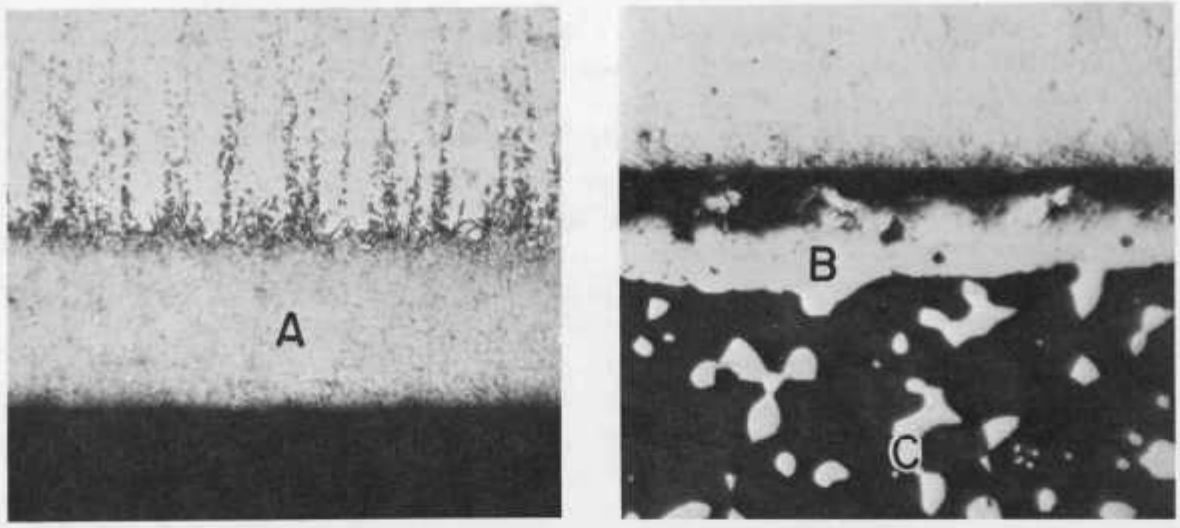

(a) Cladding Etched

(b) Fuel Etched

Fig. 22. V-15 wt % Ti-7.5 wt % Cr vs $(U,Pu)_2C_3$ after 800°C Test for 1000 hr. A is the carburized zone in the cladding, B is the (U,Pu)C zone formed by reduction of $(U,Pu)_2C_3$, and C is the (U,Pu)C impurity in the fuel. Mag. 375X. Neg. Nos. MSD-48689 and MSD-48687.

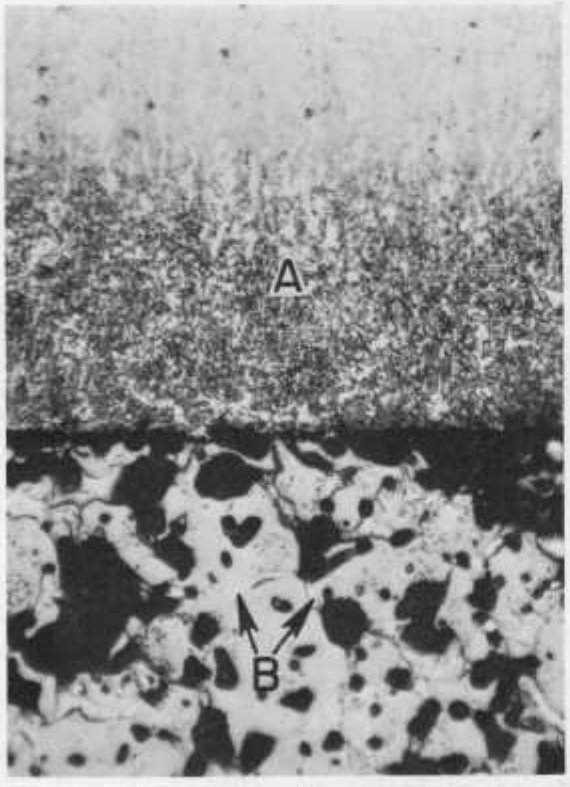

Fig. 23

V-20 wt % Ti vs (U,Pu)C after 950°C Test for 168 hr. A is the carbide precipitate zone in the cladding, and B is the (U + Pu) metal in the grain boundaries of the fuel. Mag. 375X. Neg. No. MSD-40551.

Much improved compatibility with carbide fuels resulted from a reduction of the titanium content of these vanadium alloys. No metallographic effects were observed in V-15 wt % Cr-5 wt % Ti after contact with the hyperstoichiometric (U,Pu)C for 1000 hr at 800°C. After 4000 hr at 800°C, however, an affected zone of 70 μ was revealed by etching (see Fig. 24). The microhardness of this zone was 250 DPH, compared with 198 DPH for the remainder of the cladding disk. Estimation of the carbon content of this zone by chemical analysis was 0.5 wt %.

No bulk carburization of V-10 wt % Cr was observed after contact with hyperstoichiometric (U,Pu)C for 4000 hr at 800°C. Also, no increase in hardness occurred near the interface. However, etching revealed a widening of grain boundaries of the V-10 wt % Cr after contact with hyperstoichiometric (U,Pu)C for 1000 and 4000 hr (see Fig. 25). Because of the small size of the grain-boundary phase (1-2 μ wide), quantitative analysis could not be obtained by the electron microprobe. However, microprobe results for carbon in the grain-boundary phase showed no change in intensity over that of the matrix, indicating that the phase was not a carbide and probably contained less than 1 wt % carbon. The V-10 wt % Cr alloy was similarly affected after contact with $(U,Pu)_2C_3$ for 1000 hr at 800°C. In addition to the grain-boundary effect, however, there was evidence of oxygen diffusion from the vanadium alloy to the carbide fuel. Electron-microprobe analysis revealed that a gray phase in the grain boundaries and within the grains of $(U,Pu)_2C_3$ contained oxygen, and therefore the phase was assumed to be $(U,Pu)O_2$ (see Fig. 26).

The grain boundaries of VANSTAR-7 were similarly affected after contact with hyperstoichiometric (U,Pu)C at 800°C. This alloy, composed essentially of vanadium, chromium, and iron, was affected to approximately the same depth (150 μ) as V-10 wt % Cr after 1000 hr (see Fig. 27). Also, as with V-10 wt % Cr, microhardness measurements showed no hardness increase near the interface.

No effects were observed between either VANSTAR-8 or VANSTAR-9 and hyperstoichiometric (U,Pu)C after 1000 hr at 800°C. These alloys contained 3.75 at. % of the strong carbide formers zirconium, tantalum, and niobium. After 4000 hr at 800°C, however, VANSTAR-8 was somewhat hardened to a depth of 625 μ from the interface. Hardness was 315 DPH at the interface and decreased to 275 DPH at a depth of 250 μ from the interface. The unaffected VANSTAR-8 alloy had a hardness of 202 DPH. Figure 28 shows the change in microstructure near the interface. VANSTAR-9 showed no hardness nor microstructural changes after the 4000-hr test, and, of the VANSTAR alloys, it appeared to be the most compatible with carbide fuel (see Fig. 29).

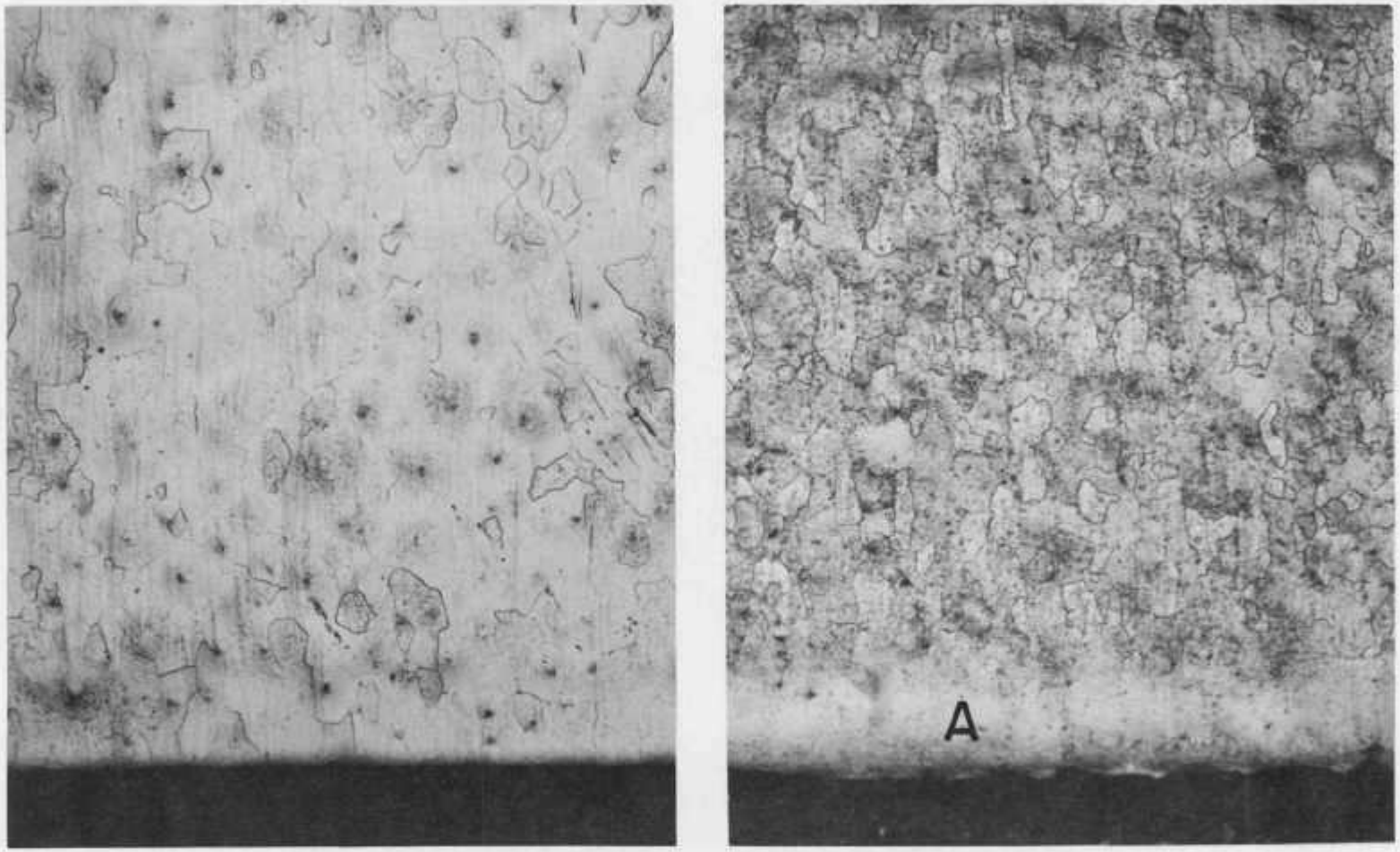

(a) 1000 hr

(b) 4000 hr

Fig. 24. V-15 wt % Cr-5 wt % Ti vs Hyperstoichiometric (U,Pu)C after 800°C Tests for 1000 and 4000 hr. A indicates the slightly hardened zone. Mag. 200X. Neg. Nos. MSD-47708 and MSD-49158.

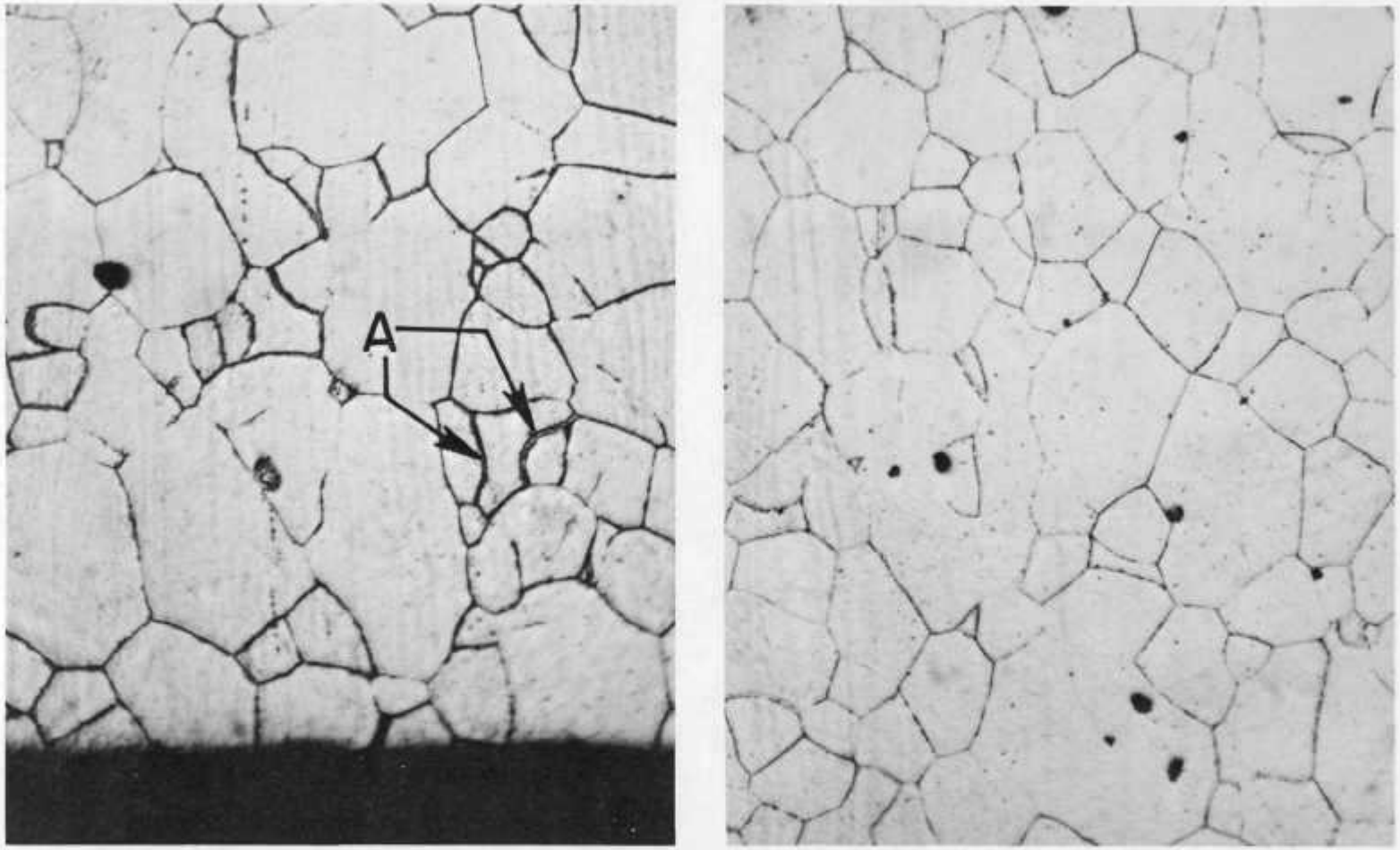

(a) Cladding at Interface

(b) Unaffected Cladding

Fig. 25. V-10 wt % Cr vs (U,Pu)C after 800°C Test for 1000 hr. A indicates the unidentified grain-boundary phase near the fuel-cladding interface. Mag. 500X. Neg. Nos. MSD-48790 and MSD-48791.

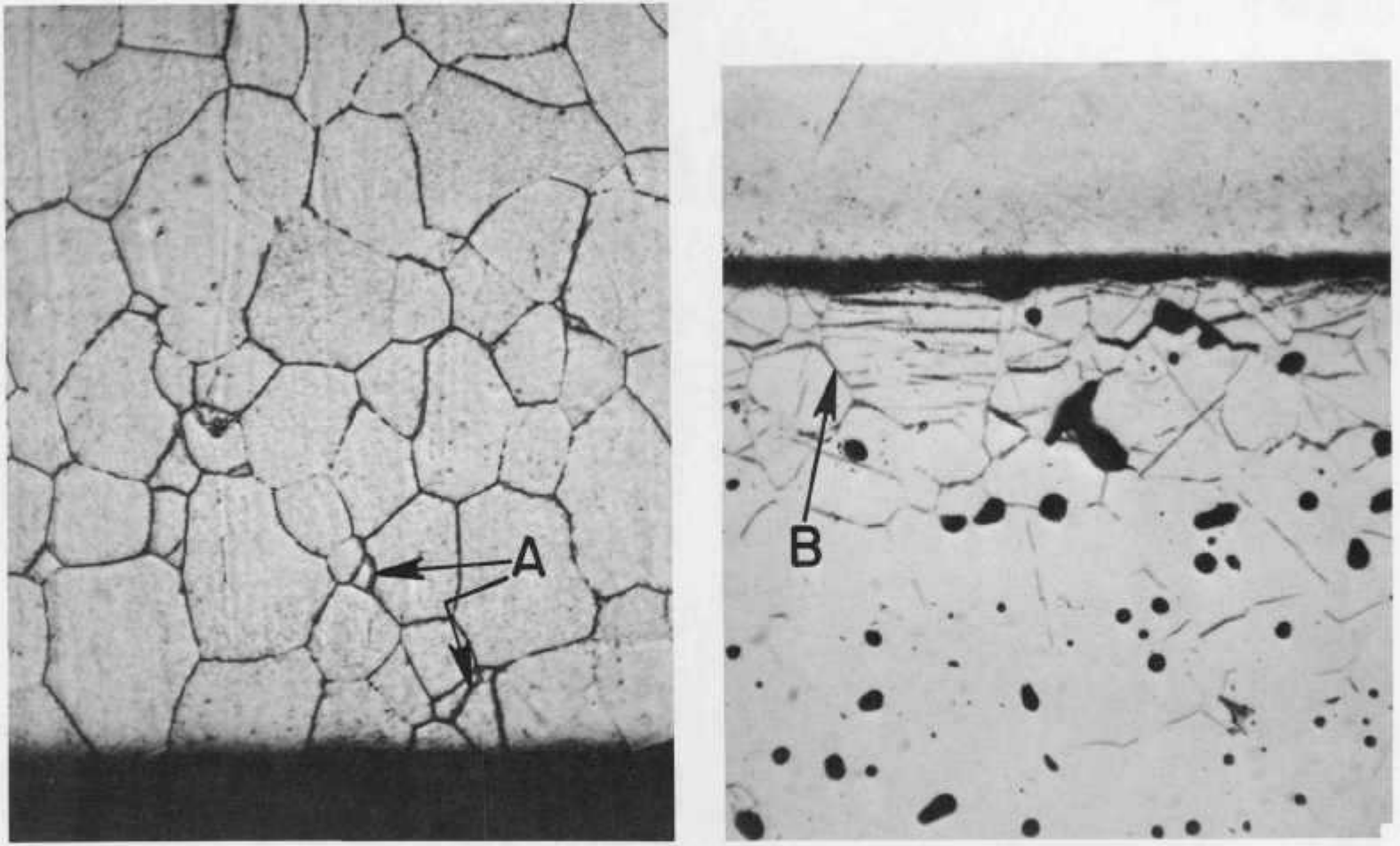

(a) (b)

Fig. 26. V-10 wt % Cr vs $(U,Pu)_2C_3$ after 800°C Test for 1000 hr. A is the unidentified grain-boundary phase in the cladding, and B is the $(U,Pu)O_2$ in the grain boundaries of the fuel. Mag. 500X. Neg. Nos. MSD-48694 and MSD-48692.

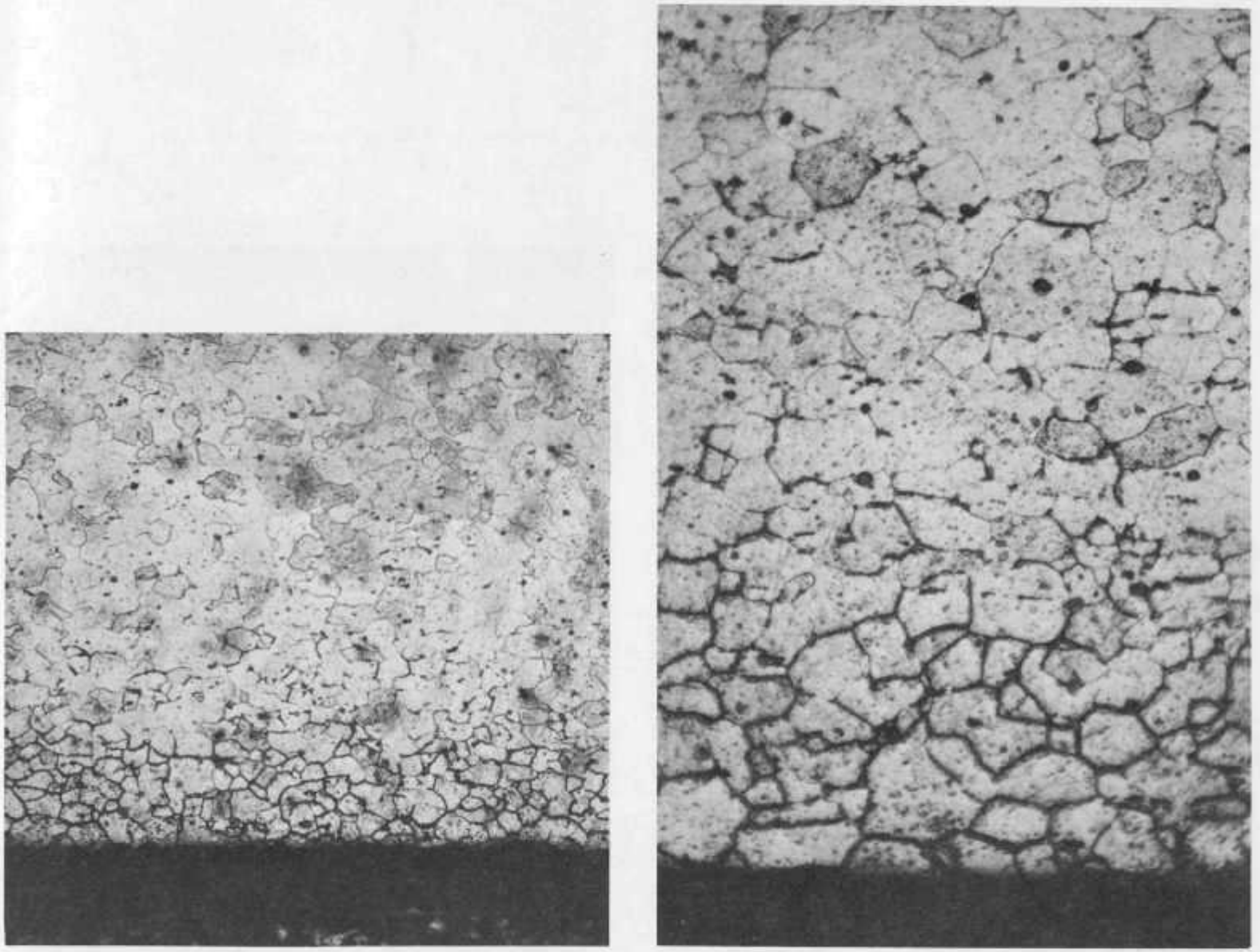

(a) 200X (b) 500X

Fig. 27. VANSTAR-7 vs Hyperstoichiometric (U,Pu)C after 800°C Test for 1000 hr. Neg. Nos. MSD-47778 and MSD-47780.

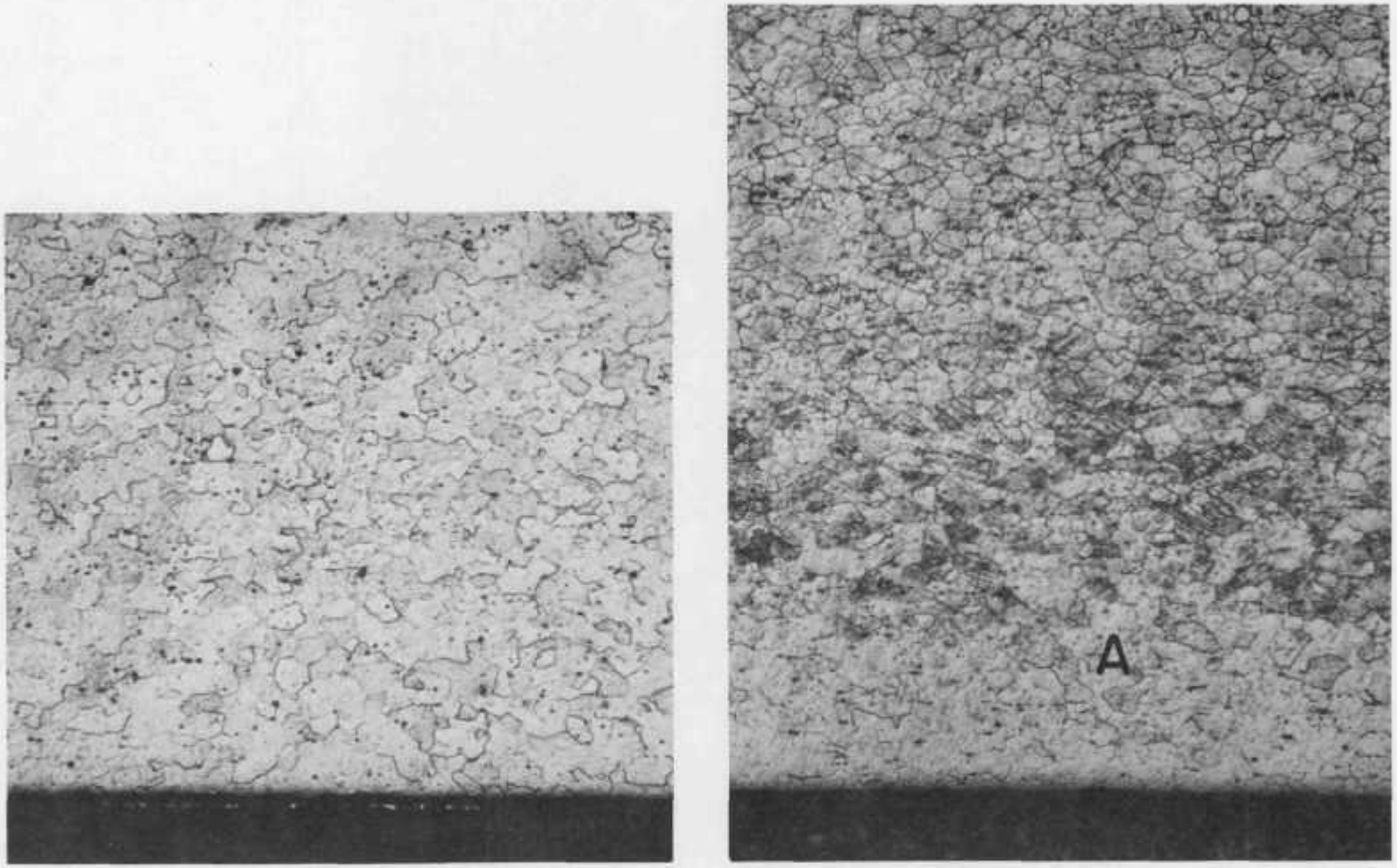

(a) 1000 hr

(b) 4000 hr

Fig. 28. VANSTAR-8 vs Hyperstoichiometric (U,Pu)C after 800°C Tests for 1000 and 4000 hr. A indicates the slightly hardened zone. Mag. 200X. Neg. Nos. MSD-47783 and MSD-54643.

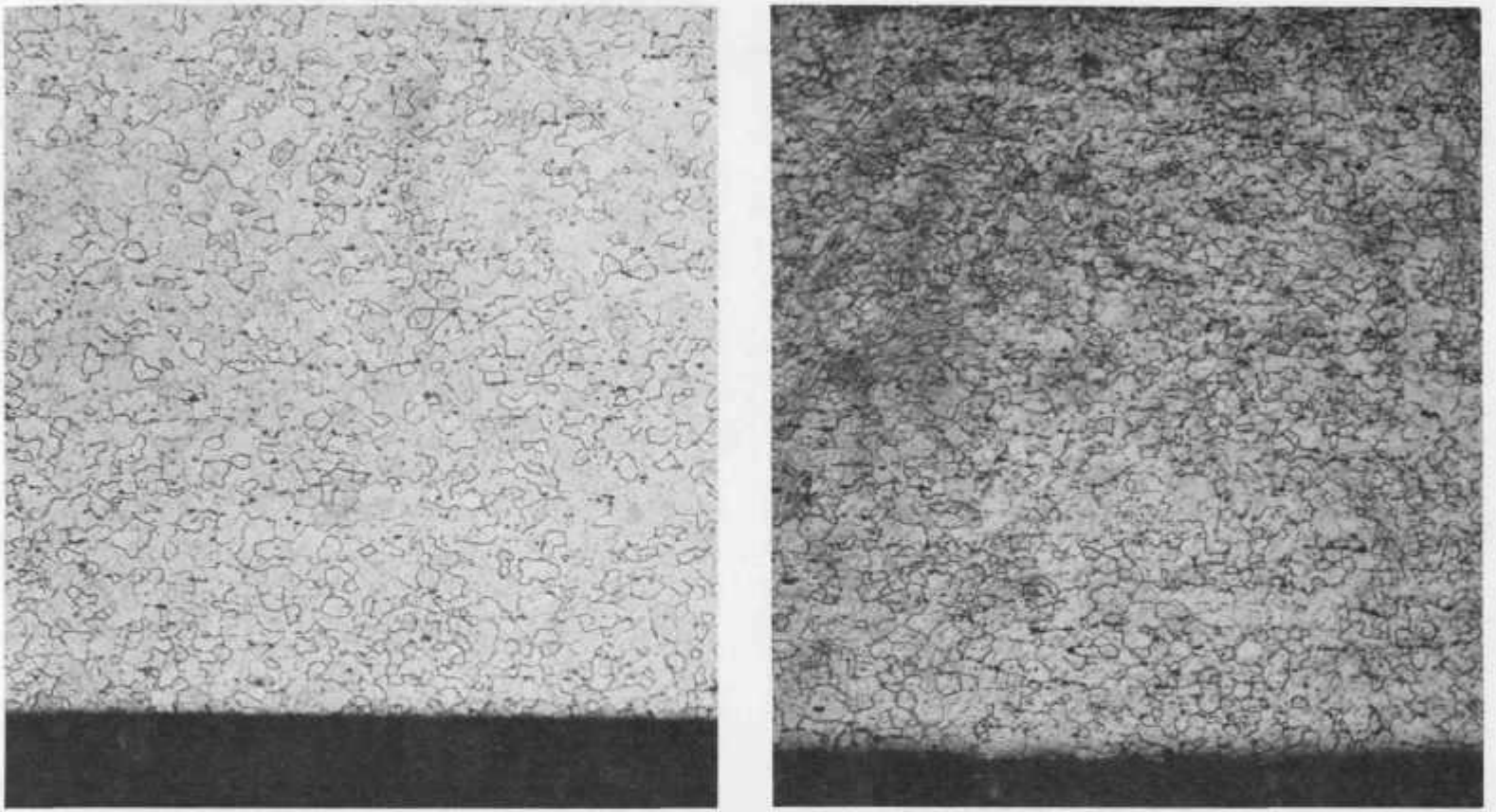

(a) 1000 hr

(b) 4000 hr

Fig. 29. VANSTAR-9 vs Hyperstoichiometric (U,Pu)C after 800°C Tests for 1000 and 4000 hr. No effects on cladding were observed. Mag. 200X. Neg. Nos. MSD-49787 and MSD-54644.

VI. CONCLUSIONS

1. Four of the five austenitic iron-base alloys containing 25 wt % or less nickel that were tested at 800°C for up to 4000 hr showed some metallographic evidence of a relatively small amount of carbon transfer from stoichiometric and hyperstoichiometric $(U_{0.8}Pu_{0.2})C$. The fifth alloy, Haynes 56, showed no metallographic evidence of carbon transfer. The carbon transfer was observed as increased precipitation of chromium-rich precipitates in Types 304 and 316 stainless steel and as molybdenum-rich precipitates in Timken alloys 16-15-6 and 16-25-6. No increase in the depth of these precipitates was observed in the Timken alloys between 1000 and 4000 hr. Determination of the depth of carbon diffusion in the stainless steels was difficult because the compressive stresses imposed upon the stainless steel specimens at the beginning of the heat treatment resulted in characteristic carbide precipitation in the slightly worked material in the bulk of the specimen. These results and results from other investigators appear to indicate that transfer of carbon from (U,Pu)C containing up to 20 vol % $(U,Pu)_2C_3$ is relatively small.

2. Three austenitic alloys containing over 30 wt % nickel reacted with stoichiometric and hyperstoichiometric $(U_{0.8}Pu_{0.2})C$ to form intermetallic compounds at the fuel-cladding interface and precipitates in the cladding at 700 and 800°C. The compound formed in the tests with Hastelloy-X and Inconel 625 was $(U,Pu)Ni_5$. Carbon released by the reaction diffused into the cladding alloys and was found as chromium- and molybdenum-rich precipitates. The depth of the intermetallic layer was relatively small for Incoloy 800 and Hastelloy-X (about 5 μ after 4000 hr at 800°C).

3. The compatibility of the vanadium alloys tested was markedly affected by the amount of titanium contained in these alloys. Vanadium alloys containing 15-20 at. % Ti were carburized by $(U_{0.8}Pu_{0.2})C$ and reduced $(U,Pu)_2C_3$ to (U,Pu)C at 800°C. However, metallography and microhardness measurements indicated that vanadium alloys containing only 5 at. % or less of titanium or other relatively strong carbide formers, such as zirconium, tantalum, and niobium, were only slightly affected by contact with hyperstoichiometric (U,Pu)C at 800°C for up to 4000 hr.

ACKNOWLEDGMENTS

I wish to thank Messrs. D. C. O'Rourke and J. A. Lahti for their assistance in preparing the compatibility specimens, and J. E. Sanecki for the microprobe data. The valuable advice and help received from Dr. C. M. Walter in the early stages of this work are also gratefully acknowledged.

REFERENCES

1. M. E. Nicholsen, C. H. Samans, and J. F. Shortsleeve, *Composition Limits of Sigma Formation in Nickel-Chromium Steels at 1200°F (650°C)*, Trans. Am. Soc. Metals *44*, 601 (1952).

2. M. Hansen, *Constitution of Binary Alloys*, 2nd ed., McGraw-Hill Book Co., New York (1958).

3. W. Batey, K. Bolton, D. M. Donaldson, and G. Yates, "Compatibility of (U,Pu) - Carbides with Cladding Materials," *Carbides in Nuclear Energy*, Macmillan and Co., Ltd., London, Vol. 1, pp. 392-402 (1964).

4. P. M. French and D. J. Hodkin, "Mechanical Properties and Compatibility of Uranium-Plutonium Carbides," *Plutonium 1965*, Chapman and Hall, London, pp. 697-720 (1967).

5. W. Batey, D. Donaldson, and G. Yates, "The Compatibility of Type 316L Stainless Steel with Mixed Uranium-Plutonium Carbides," *Plutonium 1965*, Chapman and Hall, London, pp. 888-908 (1967).

6. F. Anselin, D. Calais, and J. C. Passefort, *Etude du Diagramme Ternaire Uranium-Carbone-Nickel*, CEA-R 2845 (Aug 1965).